Decoupling the Effect of Rubbing and Annealing on The Enhanced Device Performance in Sequentially Deposited Bilayer Organic Solar Cells

Mohd Zaidan bin Abdul Aziz

Japan Advanced Institute of Science and Technology

Doctoral Dissertation

Decoupling the Effect of Rubbing and Annealing on The Enhanced Device Performance in Sequentially Deposited Bilayer Organic Solar Cells

Mohd Zaidan bin Abdul Aziz

Supervisor: Professor Dr. Hideyuki Murata

School of Materials Science
Japan Advanced Institute of Science and Technology

March 2021

Abstract

This research mainly focuses on the bilayer configuration of organic solar cells (OSCs) through layer-by-layer sequential deposition of conjugated polymer and fullerene derivative. The common Poly(3-hexylthiophene-2,5-diyl) (P3HT) and [6,6]-phenyl-C61-butyric acid methyl ester (PCBM) have been utilized as the main materials for the electron donor and electron acceptor, respectively. The bilayer device configuration enables the polymer layer to be favourably adjusted by rubbing. Rubbing on polymer layer was reported to bring about the favourable molecular orientation from edge-on to face-on that is beneficial for the charge transport in out-of-plane direction for enhanced photovoltaic performances. In this regards, the application of rubbing on conjugated polymer layers has been emphasized throughout the research work, aiming to achieve enhanced performances rubbed bilayer OSCs.

Initially, the understanding of the device fabrication procedures of the bilayer P3HT/PCBM OSCs were acquired by fabricating the unrubbed devices in as-deposited and annealed conditions. The photovoltaic performances of the devices were analysed via morphological studies (by atomic force microscope, AFM), optical studies (by UV-Vis spectrophotometer) and structural studies (by Fourier-transform infrared spectroscopy equipped with p-polarized multiple-angle incident resolution spectrometry, pMAIRS). Subsequently, the device fabrication parameters were optimized by considering the substrate cleaning, electron acceptor, P3HT solvent, heat treatment and the evaporation rate of the metal electrode. By taking into account the optimized device fabrication parameters, we managed to fabricate the unrubbed devices having reproducible photovoltaic performances.

In addition to the unrubbed OSCs, the rubbed devices were also fabricated by making use of enhanced rubbing technique. The efforts to improve the conventional rubbing technique were performed in order to acquire the quantitative rubbing parameters (i.e. rubbing pressure). An automatic rubbing device was developed to get better control of the parameters of rubbing processes. The unfavourable result of the automatic rubbing approach, however, has led to the use of the folded nylon cloth with a clip. The clipped nylon cloth enables the variation of the rubbing number at the consistent rubbing pressure. Including the abovementioned characterizations, thin film thickness measurement and compositional studies (by energy dispersive X-ray spectroscopy, EDS) have been performed to correlate the enhanced PV performances of the devices with the rubbing technique.

We have revealed the individual effect of rubbing and annealing mainly through the compositional studies and structural studies of the photoactive layers before and after annealing. While rubbing brings about the favourable vertical concentration gradient than facilitates the efficient charge transport, annealing further segregates the bilayers to form intimately large intermixed P3HT:PCBM layer for an adequate charge generation. Also, pMAIRS measurements indicates that the small change of P3HT molecular reorientation from edge-on to face-on by rubbing does not contribute to the enhanced photovoltaic performances of the devices. Therefore, the enhanced performances of bilayer OSCs before and after annealing have been confirmed to be mainly attributed by adequate vertical concentration gradient of the photoactive layers. This finding will open up the opportunity to further enhance the performances of bilayer OSCs using other electron donor and electron acceptor systems.

Keywords: Bilayer organic solar cells, rubbing, annealing, molecular orientation, vertical concentration gradient.

ACKNOWLEDGEMENTS

First and foremost, I would like to express my heartiest gratitude to Professor Hideyuki Murata and Assistant Professor Heisuke Sakai for their continuous supports and guidance throughout my research works. Also, many thanks to the staff of JAIST and all members of Murata Laboratory for their kind assistance, supports and encouragement. Not to forget, a great appreciation to Professor Keisuke Ohdaira and his laboratory members for their big help on my minor research project. We also acknowledge the generous help from Assistant Prof. Dr. Varun from University of Electro-Communications (UEC) for his kind guidance in experimental procedures to fabricate the reproducible bilayer OPV devices. Also, a special thanks to Mr. Higashimine from The Center for Nano Materials and Technology (CNMT) for his invaluable helps to measure the EDS mappings of our devices. Also, many thanks to our collaborators: Professor Hasegawa and his laboratory members for their priceless contribution in providing the guidance on the measurement of molecular orientation of our samples using pMAIRS technique. Last but not least, I have been very grateful for the prayers, concerns and continuous support from my family in Malaysia.

Table of Contents

Chapter 1: INTRODUCTION 1

1.1 Organic Solar Cells 1

1.2 Architecture of OSCs: Single Junction, Bulk Heterojunction, Bilayer, Nanostructured, Tandem 3

1.2.1 Single Layer 3

1.2.2 Bilayer 4

1.2.3 Bulk Heterojunction 6

1.2.4 Nanostructured 7

1.2.5 Tandem 8

1.3 Photovoltaic Performance Parameters of OSCs 9

1.4 Morphological, Optical, Compositional and Structural Properties of OSCs Active Layer 12

1.5 Molecular Orientation of Conjugated Polymer 12

1.6 Fabrication Process of OSCs 14

1.7 Device Performance Reproducibility of OSCs 15

1.8 Aims of study 17

1.9 Structure of Thesis 18

1.10 References 20

Chapter 2: OPTIMIZATION OF BILAYER P3HT/PCBM OSCS AND CHARACTERIZATIONS OF P3HT FILMS 23

2.1 Introduction 23

2.1.1 Bilayer P3HT/PCBM OSCs 23

2.1.2 The State-of-the-art of the Performance of Bilayer P3HT/PCBM OSCs 26

2.2 Experimental Procedures 27

2.2.1 Fabrication and PV Evaluation of Bilayer P3HT/acceptor OSCs and P3HT Film Samples 27

2.2.2 Optimization Process of OSCs Fabrication Parameters: Substrate Cleaning, Electron Acceptor, P3HT Solvent, Heat Treatment and Evaporation Rate of Al Electrode 29

2.2.3 Characterizations of P3HT Film Samples 31

2.3 Results and Discussion 31

2.3.1 Effect of Substrate Cleaning on The Photovoltaic Performance of P3HT/PCBM OSCs 31
2.3.2 Effect of Different P3HT Solvents on The Photovoltaic Performance of P3HT/PCBM OSCs 34
2.3.3 Effect of Different Electron Acceptors on The Photovoltaic Performance of Bilayer P3HT-based OSCs 36
2.3.4 Effect of Evaporation Rate of Al Electrode on The Photovoltaic Performance of P3HT/PCBM OSCs 39
2.3.5 Effect of Pre-annealing and Post-annealing on The Photovoltaic Performance of P3HT/PCBM OSCs 41
2.3.6 Performance of Optimized Bilayer P3HT/PCBM OSCs 43
2.3.7 Morphological, Optical and Structural Analyses of Optimized P3HT Films 44
2.4 Summary 48
2.5 References 50

Chapter 3: ENHANCEMENT OF PHOTOVOLTAIC PERFORMANCE OF OSCS BY RUBBING TECHNIQUE 52
3.1 Introduction 52
3.1.1 Rubbing Technique 53
3.2 Experimental Procedures 53
3.2.1 Development of Rubbing Technique 53
3.2.2 Fabrication Process of Rubbed P3HT Films and P3HT/PCBM OSCs 55
3.3 Results and Discussion 56
3.3.1 Effect of Rubbing by Folded Nylon Cloth and Rubbing Tool 2 on The Photovoltaic Performance of P3HT/PCBM OSCs 56
3.3.2 Effect of Different Rubbing Pressures by Manual and Automatic Rubbing on The Photovoltaic Performance of Bilayer P3HT/PCBM OSCs 59
3.3.3 Effect of Rubbing by Clipped Nylon Cloth on The Photovoltaic Performance of P3HT/PCBM OSCs 63
3.4 Summary 65
3.5 References 67

Chapter 4: REPRODUCIBLE DEVICE PERFORMANCE AND EFFECT OF RUBBING ON THE PERFORMANCE OF P3HT/PCBM OSCS 69
4.1 Introduction 69
4.1.1 Factors Causing the Poor Device Performance Reproducibility 69
4.1.2 Vertical Concentration Gradient and Molecular Orientation on BL P3HT/PCBM OSCs 70
4.2 Experimental Procedures 70
4.2.1 Fabrication Process of Reproducible P3HT/PCBM OSCs 70
4.2.2 Fabrication Process and Characterizations of Rubbed P3HT/PCBM OSCs and P3HT Films 71
4.3 Results and Discussion 72
4.3.1 Photovoltaic Performance of Reproducible Unrubbed P3HT/PCBM OSCs 72
4.3.2 Photovoltaic Performance of Rubbed P3HT/PCBM OSCs 75
4.3.3 Morphological, Compositional and Structural Properties of Unrubbed and Rubbed Active Layers 76
4.4 Summary 84
4.5 References 86

Chapter 5: CONCLUSION AND FUTURE WORKS 88
5.1 Conclusion 88
5.2 Future Works 89

Chapter 1

INTRODUCTION

1.1 Introduction

1.1.1 Organic Solar Cells

The civilization and modernization have been facilitating the life of human beings with the invention of various devices, machines, transports and skyscrapers. Despite of this outstanding achievement, the energy scarcity has been threating the mankind day by day, giving rise to the awareness of seeking the new and long-lasting energy source. One of the feasible efforts to overcome this issue is the invention of photovoltaic (PV) cells which is a kind of renewable energy source that utilizes the direct sunlight as the energy source to induce the electricity.[1] The operation mechanism of the PV cell via photoelectric effect was firstly applied on crystalline silicon (c-Si) PV cell which has been regarded as the first generation PV cell.[1,2] Since the commercialization of the first generation PV cells made by c-Si, the research and development on PV cells have been developing with the emergence of the second generation PV cells based on inorganic semiconductor materials (e.g. amorphous Si, II-VI group semiconductors such as CdS and CdTe).[3] This kind of PV cells uses thin film deposited on the substrate with cost-effective fabrication technique and flexibility up to a certain degree instead of costly and bulky c-Si modules.[4]

Third generation PV cells that consist of dye-sensitized solar cells, organic solar cells (OSCs) and perovskite PV cells have been developed by employing more environmental-friendly fabrication processes and materials.[5] Since the last few decades, OSCs have been the well-known research topic with tremendous attention owing to their advantages being transparent, flexible, low cost, lightweight and feasible large-scale deposition at low

temperature.[6–8] The extensive research progress has been improving the performance of OSCs in which the current state-of-the-art (Figure 1) shows that the OSCs have achieved the power conversion efficiency (*PCE*) over 17 % with the use of high performance donor-acceptor materials, well-designed architecture and optimized experimental procedures.[9–15]

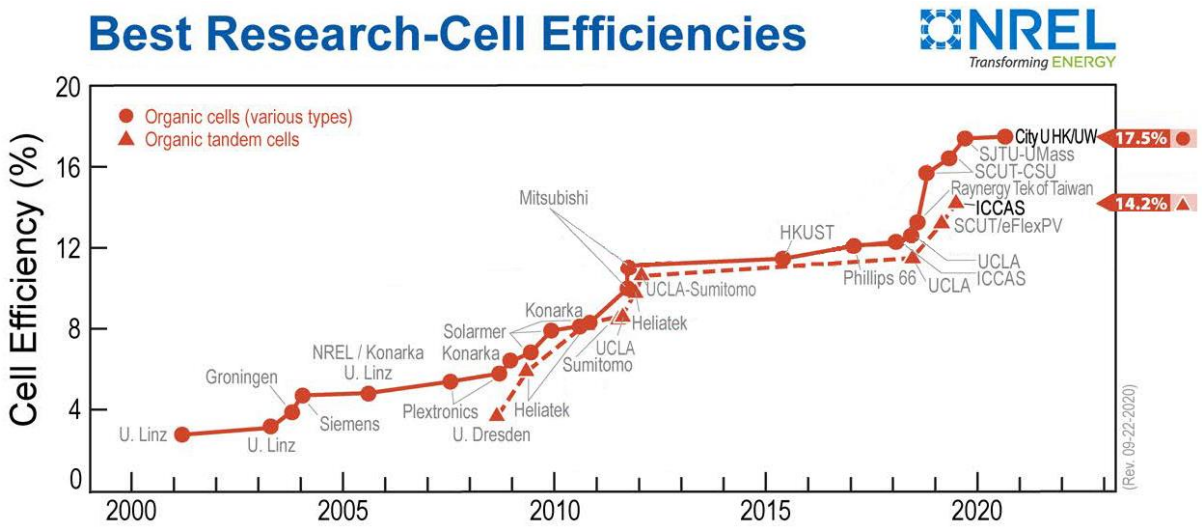

Figure 1.1. The current state-of-the-art of OSCs.[16]

Basically OSCs are made up of donor material of either small molecules or conjugated polymers and acceptor material such as fullerene derivative.[17] The capability of these organic materials to be deposited by solution process on the transparent and flexible substrates[18,19] has broaden the possible application of the fabricated devices on rooftop applications, buildings, public area and vehicles. Poly(3-hexylthiophene-2,5-diyl) (P3HT) and phenyl-C_{61}-butyric acid methyl ester (PCBM) have been the well-known representative conjugated polymer and fullerene derivative for OSCs respectively.[20,21] Basically, P3HT monomer is composed of a single hexyl chain and thiophene ring.[11] The repeating units of P3HT are symmetric with the three relative orientations consisting of head-to-tail (HT), head-to-head (HH) and tail-to-tail (TT) couplings.[22] As shown in Fig. 1.2, depending on the symmetry in the direction of the backbone, the regioregularity (RR) of P3HT can be classified as high, low or random.[22] RR is

related to the crystallinity of the polymer active layer which is an important factor that affects the performance of fabricated OSCs.[23]

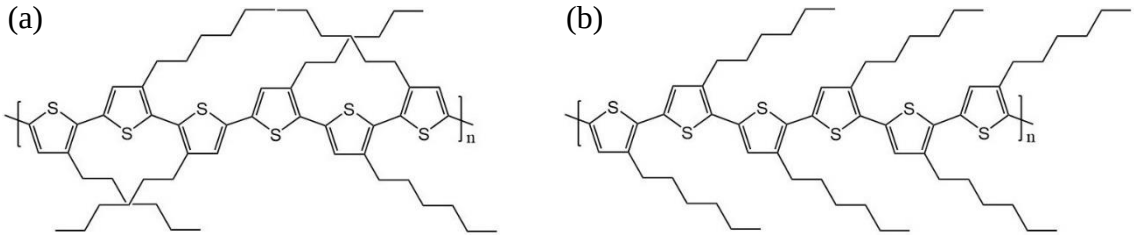

Figure 1.2. (a) Low regioregularity P3HT and (b) high regioregularity P3HT.

Depending upon the preparation of the donor and acceptor solutions, OSCs can be fabricated in various architectures including single junction, bulk heterojunction (BHJ), bilayer (BL), nanostructured and tandem. Various solution processes including screen printing, inkjet printing, doctor blading and spin coating are applicable to realize the active layers of OSCs. The selection of device architecture and solution process is based on the scale and purpose of device fabrication.

1.2 Architecture of OSCs: Single Junction, Bulk Heterojunction, Bilayer, Nanostructured, Tandem

1.2.1 Single Layer

The simplest form of OSCs were fabricated in single layer architecture (Fig. 1.3) by sandwiching a layer of an organic small molecules or polymer layer between two conductors typically a layer of transparent indium tin oxide (ITO) with high work function and a layer of low work function metal such as aluminum , magnesium or calcium.[24]

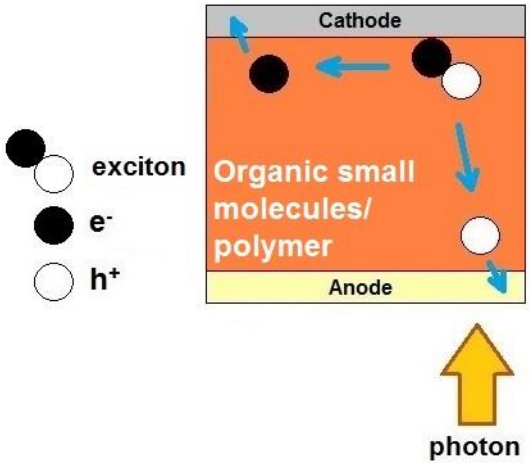

Figure 1.3. The architecture of single layer OSCs.

As the organic layer absorbs light, the excitons which are the strongly bounded electron-hole pairs are formed. The potential generated by the different work functions of transparent and metal electrodes helps to split the excitons, extracting electrons to cathode and holes to anode. Despite of this working mechanism, this single layer or homojunction OSCs does not perform well where its PCE remains below 0.1%.[2,25] A major problem with this OSCs is the electric field resulting from the difference between the two electrodes is often insufficient to split the excitons, leading to the recombination of electrons and holes prior to reaching the electrode.[2]

1.2.2 Bilayer

The BL OSCs which are also known as planar donor-acceptor heterojunction consists of two layers sandwiched between the transparent and metal electrodes as illustrated in Fig. 1.4.[2,22] Basically the active layer consists of electron donor and acceptor layers which are sequentially deposited. Therefore, the control of the properties of individual active layer (typically the donor layer) can be realized by the application of this architecture.[21,26] The appropriate materials are selected so that the local electric field is strong enough to efficiently split the excitons.[2] The

diffusion length of excitons in organic electronic materials is typically in the order of 10 nm.[27] Therefore, the thickness of the donor layer should be in the similar range so that most excitons can diffuse to the interface of layers and subsequently split into charge carriers.

This configuration is regarded as the basic concept to explain the operation mechanism of OSCs with donor and acceptor components. Upon the photon absorption in organic material, the excitons are produced.[3] The internal electric field provided by the difference of the work functions of electrodes is often insufficient to separate these photogenerated excitons to free charge carriers.[2] As a result, these excitons diffuse to the donor/acceptor heterojunction.[3] At the interface, the resulting potentials due to the difference in electron affinities (EA) and ionization potentials (IP) are strong and may induce exciton dissociation provided that the potential energy difference is larger than exciton binding energy.[17] Subsequently, the free carriers are transported to the respective electrodes with the aid of internal electric field and driven to the external circuit.[3] The separation of the excitons at donor/acceptor interface is much efficient than that of organic material/metal interface in the single layer OSCs.[2] This explains why the performance of BL OSCs is relatively better than that of single cell.

Based on the conventional BL device architecture (Fig. 1.4a), the sequential deposition of donor and acceptor via solution process enables the formation of larger donor/acceptor heterojunction (Fig. 1.4b) known as graded BL which is favorable for efficient charge generation in the active layer.[26] This structure requires careful selection of the solvent for donor and acceptor so that the deposition of the top layer does not completely destroy the bottom layer.[27,28] In this regard, chlorobenzene (CB) and dichloromethane (DCM) solvents are used to dissolve the respective P3HT and PCBM to fabricate the BL P3HT/PCBM device.[21,26] The ideally optimal active layer morphology does not only require interpenetrating networks of donor/acceptor heterojunction, but also an optimized vertical donor/acceptor composition gradient to realize efficient charge transport.[29] The proper control of the properties of P3HT layer was reported to produce the BL P3HT/PCBM with ca. 4% *PCE* which is comparable to

that of P3HT:PCBM BHJ devices.[21,30] Recently, the use of high performance copolymer, namely poly[2,7-(9,9-dioctyl-dibenzosilole)-alt-4,7-bis (thiophen-2-yl) benzo-2,1,3-thiadiazole] (PSiF-DBT) and C70 fullerene to form the BL OSCs yield up to 5.75% *PCE*.[31] This shows that this kind of OSC has the potential to be further improved with the proper control of its properties (i.e. donor-acceptor materials etc.).

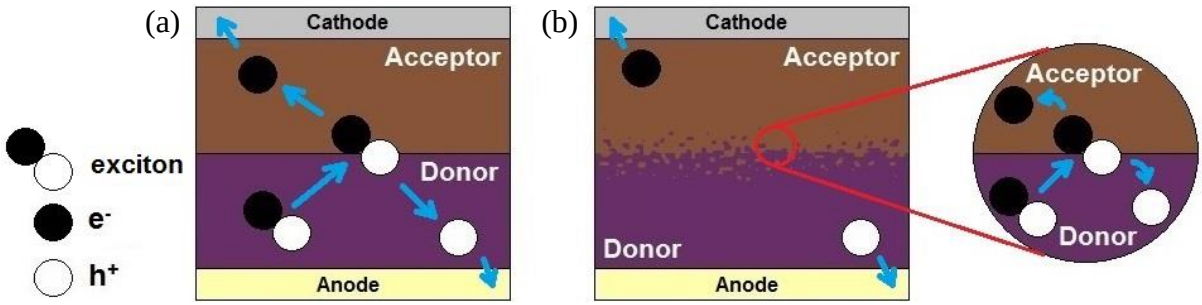

Figure 1.4. The architecture of (a) conventional (b) graded BL OSCs.

1.2.3 Bulk Heterojunction

The advancement of the OSCs fabrication has been going on with the emerging of bulk heterojunction (BHJ) device geometry. Unlike BL OSCs that uses separate donor/acceptor layers, BHJ architecture consists of the bi-continuous network of donor-acceptor nanoscale blend in a single layer[2] as shown in Fig. 1.5. The presence of the large donor-acceptor interfacial area allows the excitons with short lifetime to seamlessly reach the interface, resulting in high charge generation rate for decent performance BHJ OSCs.[18,32] The efficient BHJ layer requires to maintain large enough domain size to form a percolating network that allows the donor and acceptor materials to reach the corresponding electrodes for efficient charge transport. It was reported that the control of active layer growth rate has realized the BHJ P3HT:PCBM device with 4.4% *PCE*.[33] The drawback of this configuration is that the random blend of active layer partially causes the charges to travel for a long distance before

reaching the electrode which in turn results in charge recombination.[27] Despite such limitation, the use of high-end material (i.e. gold nanoparticles) with the high performance active materials for BHJ OSCs has realized the decent *PCE* of 9.89%.[15]

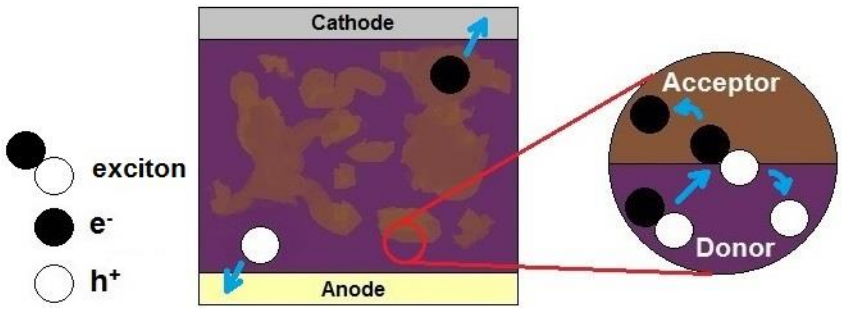

Figure 1.5. The architecture of bulk heterojunction OSCs.

1.2.4 Nanostructured

It is believed that vertical composition gradient and inter-digitated nanostructures can form optimum heterojunction structure.[34] In this regard, the nanostructured OSCs (Fig. 1.6) was designed to overcome the charge recombination issue of BHJ device and simultaneously maintain the exciton dissociation.[34,35] This kind of OSCs applies the specific design principles to maximize the exciton dissociation. Apart from nanoimprint lithography, self-assembly with polystyrene is used to form the inter-digitated pattern.[36] This periodic pattern is designed to comply with the exciton diffusion length which is in the order of 10 nm.[27] The height of the pattern needs to be tuned to absorb sufficient photons with minimal charge recombination.

The refraction of light in the patterned active layer enhances absorption of light due to longer travel distance of incident light. Hence, there is higher probability of exciton formation in the active layer. The large donor-acceptor interface enables the dissociation of photogenerated excitons and subsequently the arrays of nanostructures allow the dissociated charges to diffuse towards their corresponding electrodes.[34] The high probability of exciton

formation and the large area at donor-acceptor interface has realized the nanostructured P3HT/PCBM OSCs with 3.25% *PCE*.[30]

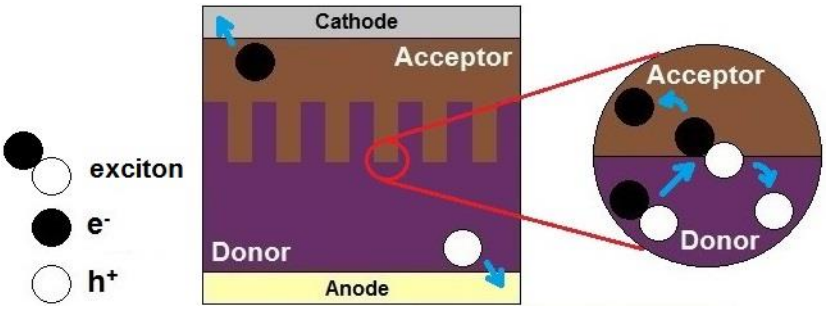

Figure 1.6. The architecture of nanostructured OSCs.

1.2.5 Tandem

As shown in Fig. 1.7, tandem OSCs are fabricated by stacking at least one device on top of another device in which each device contains the component that complements the absorption spectra. The piled devices are composed of a donor-acceptor component each. This configuration is developed to tackle the limitation of single junction OSCs that has narrow absorption due to restricted thickness of donor layer.[13] The photon which is not absorbed in the bottom device can penetrate into the top device. The two cells are connected by an intermediate layer that functions to allow the recombination of the holes from one device with electrons from the other device.[17] The intermediate layer should confirm the alignment of the quasi-Fermi level of the acceptor of the bottom device with the quasi-Fermi level of the donor of the top device.[13]

The efforts to improve the performance of tandem OSCs include the application of different fabrication techniques, novel materials, various device structures and interstitial layers. The *PCE* of tandem OSCs can be enhanced by properly matching the individual devices to create spatial separation of the separate absorption of high-energy photons and low-energy photons.[37]

The recent vacuum-processed tandem OSCs has reached an unprecedented record *PCE* of 18.6% with the use of high performance electron donor and acceptor materials for the top and bottom device.[38]

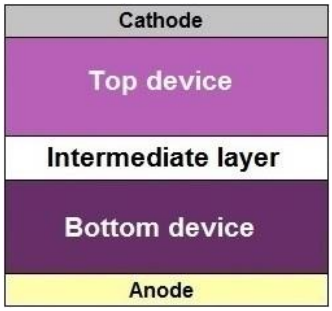

Figure 1.7. The architecture of tandem OSCs.

1.3 Photovoltaic Performance Parameters of OSCs

OSCs are characterized under a 100 mW cm^{-2} light (AM1.5G) matching the spectrum of the sun to the earth's surface (Fig. 1.8a).[39] The typical current density-voltage (*J*-*V*) curves of a solar cell in the dark and under illumination is shown in Fig. 1.8b. In the dark condition, there is almost no flow of current until the forward bias for voltage is larger than open circuit voltage.[40]

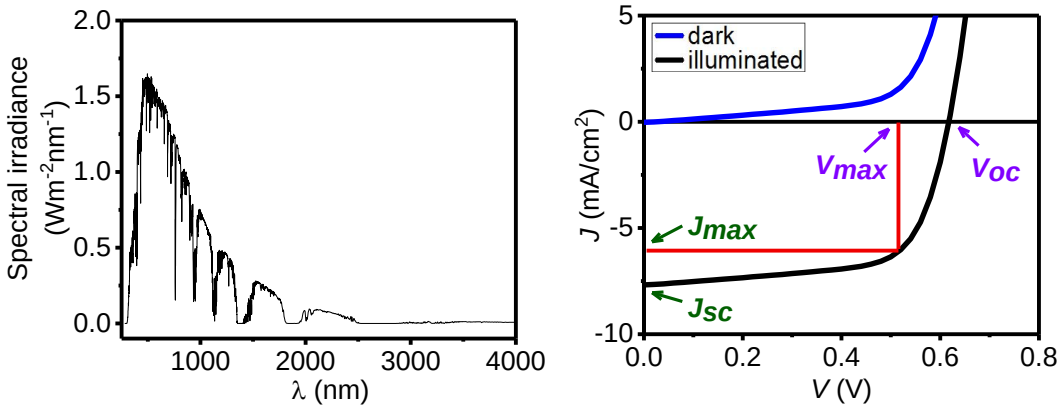

Figure 1.8. (a) The standard AM1.5G solar spectrum[41] and (b) the typical J-V curves of an organic photovoltaic cell under dark and illuminated conditions.

The generated power under illuminated condition can be measured using a solar cell simulator. The most important parameter to determine the performance of OSCs is *PCE* which can be derived as follows.[42]

$$PCE = \frac{I_{sc} \times V_{oc} \times FF}{P_{in}} \tag{1.1}$$

Short circuit current, open circuit voltage, fill factor and incident light power density are abbreviated as I_{sc}, V_{oc}, FF and P_{in} respectively. I_{sc} is the current flow through the photovoltaic cell without an external load.[43] This PV characteristic has been commonly converted as short circuit current density (J_{sc}, in mA/cm^2). I_{sc} is determined by the product of the photoinduced current density and the charge carrier mobility in the organic active layer as follows.

$$I_{sc} = ne\mu E \tag{1.2}$$

n, e, μ and E are defined as the density of charge carrier, elementary charge, mobility and electric field respectively. To obtain high density charge carrier, a small bandgap organic layer is used to harvest a broad solar spectrum. As J_{sc} is related to spectral response, it can also be calculated by integrating the external quantum efficiency, η_{EQE} against AM 1.5G spectrum (Fig. 1.8).[13]

$$J_{sc} = e\int_{E_g}^{\infty} \eta_{EQE}(E) n_{AM1.5}(E) dE \tag{1.3}$$

e is the elementary charge (1.6×10-19 C), $n_{AM1.5}$ is photon flux density on the surface of earth under AM1.5 illumination, E is photon energy and E_g is the bandgap energy of the donor material. From Equations 1.2 and 1.3, J_{sc} is known to be proportional to the number of absorbed

photons[43] and also serves as a good indicator of charge recombination.[17] V_{oc} is described as the voltage which compensates the current flow through the external circuit.[43] In OSCs, V_{oc} is linearly correlated to the difference between the HOMO energy level of the donor ($E_{HOMO,\,D}$) and LUMO energy level of the acceptor ($E_{LUMO,\,A}$) with the presence of Ohmic contact between the photoactive layer and electrodes.[17] The empirical relationship between these energy levels and V_{oc} can be drawn as follows.[39]

$$V_{oc} = \frac{1}{q}\left(E_{HOMO,D} - E_{LUMO,A} - 0.3V\right) \tag{1.4}$$

From the equation above, 0.3V accounts for the empirical energy lost during the photo-induced charge-generation process.[44] The morphology at polymer/fullerene heterojunction can also influence the V_{oc} as the work functions of the electrodes are modifiable at the interface. The charge recombination can also induce the V_{oc} loss.[39] On the other hand, fill factor (*FF*) is defined as the ratio between the maximum power (P_{max}) and the product of V_{oc} and I_{sc} as in the equation below.[42]

$$FF = \frac{V_{max} \times I_{max}}{V_{oc} \times I_{sc}} \tag{1.5}$$

P_{max} is the product of maximum voltage (V_{max}) and maximum current (I_{max}) which are illustrated in Fig. 1.9. The competition between the recombination and transport of the charge carriers affects the *FF*. In other words, *FF* can be thought as how easy the photogenerated carriers can be extracted from the device.[43] The explanation of these PV characteristics serves as a guidance on how to design the decently performed OSCs.

1.4 Morphological, Optical, Compositional and Structural Properties of OSCs Active Layer

The PV performance of OSCs is closely related to the properties of the photoactive layers that can be revealed via morphological, optical, compositional and structural analyses. These properties influence the functionality and performance of OSCs. The morphology of OSCs active layer is measured to reveal the surface roughness and thickness of the deposited polymer films. The morphology of active layer is usually altered to obtain the large area of donor/acceptor interface for better exciton dissociation and charge generation.[26,36] Optical studies involves the interaction of light (photon) with the organic thin films through absorbance, transmission or reflectance. The understanding of this characteristic helps to predict the quality of active layer against the spectral response.

The elements that make up the device active layer is investigated via compositional studies. The elemental distribution confirm the phase formation once the active layer properties (e.g. morphology or crystallinity) is altered. Structural studies is employed to evaluate the crystallinity and molecular orientation of conjugated polymer.[23] This characteristic is related to the charge transport in the active layer which takes place in vertical direction in case of OSCs. The morphological, optical, compositional and structural properties of the deposited active layers are known to be inter-related in which they have been researched to enhance the current performance of OSCs. The understanding of these properties is essential to reveal the drawback of the fabricated PV devices and simultaneously realize the devices with decent performance.

1.5 Molecular Orientation of Conjugated Polymer

The charge transport in OSCs takes place in vertical direction which is perpendicular to the substrate.[21] Therefore, the molecular orientation of conjugated polymer is essential in assisting

the charge transport in OSCs active layer. The typical conjugated polymer for OSCs, P3HT is made up of alkyl chain and thiophene ring.[45] The molecular orientation of this conjugated polymer is characterized through the change in the orientation of thiophene ring.

There are a few applicable methods to orient the polymeric molecules including off-center spin coating[29,46], dipping, nano-confinement[47], friction transfer, applied electric field, slide coating, epitaxy, strain, Langmuir-Blodgett and rubbing.[21,23] Among these methods, rubbing is known as an easy technique for the molecular orientation of polymer film.[21] It has been demonstrated that rubbing P3HT prior to electron acceptor deposition as depicted in Fig. 1.9a can enhance the performances of annealed (AND) BL OSCs through the formation of adequate donor–acceptor vertical concentration profiles.[21] Apart from that, such application of pressure on the electron donor layer at a certain direction by rubbing has been reported to be effective in aligning the molecular orientation of P3HT molecules from edge-on to face-on (Fig. 1.9b and c) which is favorable for efficient transport of charges to respective electrodes (in out-of-plane direction).[21,48]

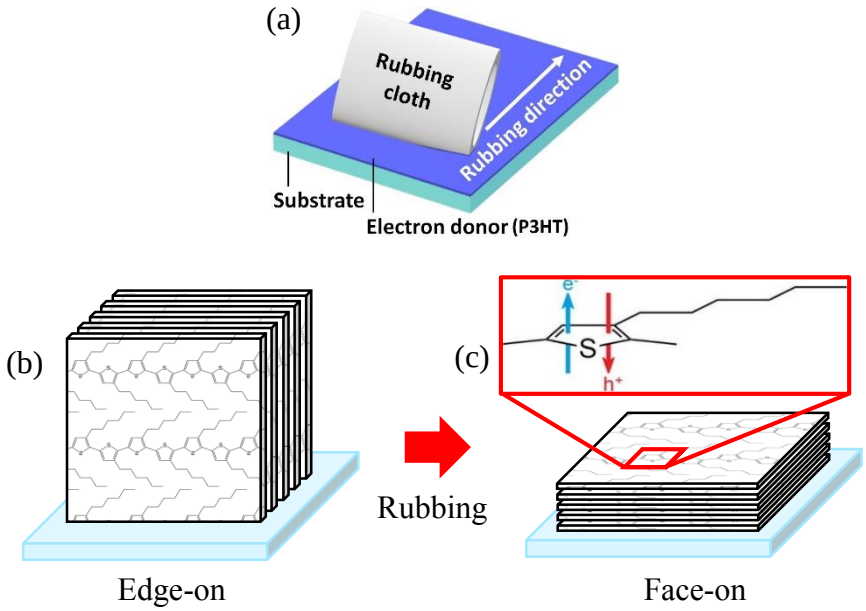

Figure 1.9 (a) Rubbing the P3HT layer prior to electron acceptor deposition. The molecular orientation schematic of (b) unrubbed (edge-on) and (c) rubbed (face-on) P3HT films.[21]

1.6 Fabrication Process of OSCs

OSCs have been commonly fabricated by solution processes in addition to the solid state process (i.e. vacuum evaporation).[42] At large scale, the solution processes take place via printing technologies and roll-to-roll (R2R) processes such as screen printing and inkjet printing.[49] These processes have been attracting substantial attention for organic electronics due to their potential low-cost processing and high volume production. At laboratory scale, the solution processes such as screen printing, doctor blading and spin coating have been employed to fabricate the devices for research purpose.

Screen printing (Fig. 1.10b) is a very versatile printing technique that can form two-dimensional patterning of the deposited layer.[37] Not only cost-effective, the application of this technique also does not inflict loss of coating solution during printing. Using a high viscosity and low volatility coating solution, it can deposit a wet film over a large area.[50] To fully make use of this process, there are several issues that need to be properly addressed including the interconnection, lifetime and mechanical stability.[17]

Based on the typical inexpensive inkjet printer, inkjet printing (Fig. 1.10b) was developed as a novel process that is applicable for industrial printing and coating.[49] The thin film deposited by inkjet printing has the common features such as continuous and pinhole-free due to the agglutination of the separately deposited ink droplets.[51] A balance between ink viscosity and surface wetting produces smooth film characterized by its low surface roughness. The high regioregular P3HT is not suitable for inkjet printing at room temperature as the fast formation of aggregates shortens the shelf life of the ink resulting in low reliability of the printing process. Having said that, the use of such P3HT forms inhomogeneous and very rough film that can detrimentally reduce the device performance.[17]

Blade coating (Fig. 1.10c) allows the firm film formation with a well-defined thickness. This deposition technique is simple and economical where the loss of coating solution can be

minimized less than ca. 5%. A so-called light soaking method was reported to improve the photovoltaic performance for blade-coated OSCs prepared with co-solvent by adjusting the P3HT surface concentration ratio for smoother carrier transport.[17,52]

Spin coating (Fig. 1.10d) is the well-known and important film-forming technique to fabricate the OSCs at a small scale, typically for research purpose. This process forms highly reproducible films that is very homogenous over the large area.[42] The maximum diameter of the substrate area that can be deposited using this process is 30 cm to homogenously dry right after the spin coating process.[17] The deciding process parameters include solution concentration, rotational speed and spin coating time.

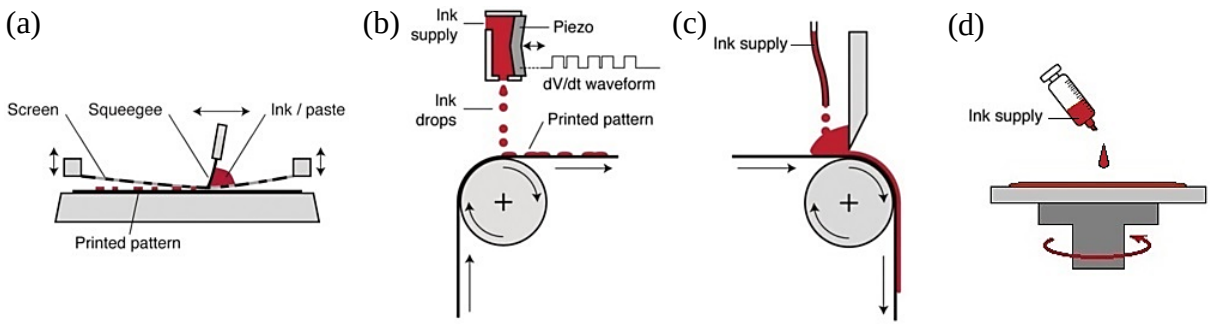

Figure 1.10 Schematic diagrams of (a) screen printing, (b) inkjet printing, (c) blade coating and (d) spin coating.[53]

1.7 Device Performance Reproducibility of OSCs

The sequential deposition of diffusive P3HT/ PCBM BL OSCs provides the possibility to independently tune the properties of each layer.[54] Unlike BHJ active layer that relies on highly unstable donor/acceptor intermixed networks and involve difficult controlling of its nanomorphology,[55] the separated BL configuration is much more attractive for more reproducible OSCs. The reproducibility of the PV performance OSCs is one of the critical issues that must be resolved prior to further investigation using high performance donor

materials. The *PCE* is a representative parameter that has been used to evaluate the performance of OSCs.[3] In addition to J_{sc}, V_{oc} and *FF*, this PV parameter is mainly used to compare the reproducibility of the OSCs. The *PCE* must be accurately measured to fairly compare the device performance. In the beginning, it could be very challenging to obtain the reproducible *PCE* with low standard deviation. The establishment of highly reproducible PV performance of OSCs requires tremendous trial and error experiments and tedious investigations to find out the possible reasons behind the non-reproducible device.

Thought the individual device is composed of identical structure and composition, there are numbers of subtle parameters that can influence its reproducibility, including the solution concentration and the presence of oxygen and moisture. Unlike the inorganic PV devices, the fabrication of OSCs via solution processes requires very careful experimental handling to achieve the reproducible devices having comparable PV performances within different batches.[56] In case of polymeric donor layers, the control of the oxygen exposure and diffusion of acceptor layer is essential to prevent the degradation of the finished device. This tricky part demands sufficient experience in device fabrication procedures including the handling of organic solvents in the nitrogen-filled glove box.

The active layer of OSCs mainly consists of the electron donor and acceptor materials where the crystalline and amorphous regions co-exist. These constituents that govern the morphology and composition of active layer are believed to induce poor reproducibility of OSCs. The analysis of the factors that contribute to poor device reproducibility and the application of consistent procedures throughout the device fabrication are anticipated to overcome the large performance variation among the OSCs.

1.8 Aims of Study

Using P3HT and PCBM as the conjugated polymer and fullerene derivative components, optimization of the BL OSCs fabrication procedures will be performed by taking into account the parameters such as substrate cleaning, acceptor selection, spin coating, solution preparation, heat treatment and evaporation rate of electrode. The performance of the optimized OSCs is aimed to be further improved by adjusting the donor layer via rubbing technique. The use of simple rubbing technique on the P3HT conjugated polymer is proven to enhance the performance of the fabricated BL device with the best PCE close to 4% and comparable to the regular P3HT:PCBM BHJ OSCs.[21,34] In this regard, further investigation on the device performance will be performed by making a good use of rubbing technique.

The conventional rubbing technique will be enhanced to provide the reproducible performance of rubbed OSCs. Also, the additional rubbing parameters will be explored to gain more control of the rubbing process. By employing the enhanced rubbing technique at the optimized experimental conditions and rubbing parameters, the PV performance of the rubbed OSCs is expected to be relatively higher than that of the unrubbed OSCs. Also, the decent and reproducible PV characteristics including J_{sc}, V_{oc}, *FF* and *PCE* are expected. One of the objectives of this research is to investigate the mechanism of the enhanced photovoltaic performance of the rubbed OSCs through the compositional, morphological and structural studies. The correlation between the PV characteristics of the devices and the aforementioned characterizations would lead to more understanding on the BL OSCs having regular device configuration.

Another objective of this research is to confirm whether the enhanced thin film properties should be attributed to rubbing, annealing or a combination of both processes as the reported study of BL OSCs was limited to annealed devices. The investigation of the individual impacts of rubbing and thermal annealing on the vertical organization of the active materials in regular

architecture BL OSCs will be performed extensively to gain in-depth understanding on the major contributing factors on the enhanced OSCs performance. As the adequate concentration profiles are the key factor to potentially extend the use of rubbing to other donor/acceptor systems, this research involves the evaluation whether such profiles formed prior to annealing.

1.9 Structure of Thesis

This thesis comprises six chapters altogether with four main parts: characterizations of the active layers, optimization of device fabrication parameters, application of rubbing technique and reproducible device performance. Each part is subsequently elaborated in a single chapter.

Chapter 1 highlights the introduction of the OSCs that includes the explanation of the device architectures, photovoltaic performance parameters, properties of active layer, molecular orientation of conjugated polymer, device fabrication processes and device performance reproducibility. This chapter includes the aims of the research as well.

Chapter 2 discusses the optimization of device fabrication parameters that involves the substrate cleaning, electron acceptor, spin coating speed, P3HT solvent, heat treatment and evaporation rate of Al electrode. This chapter also elaborates the analyses of the active layers through morphological, optical, compositional and structural studies. These characterizations are performed to understand the properties of the as-deposited (ADP) and AND donor layers before utilizing the rubbing technique.

In chapter 3, the development of rubbing technique and its application to improve the PV performance of OSCs are discussed. The use of automatic rubbing technique to control the rubbing speed and pressure is also emphasized in this chapter.

On the other hand, this Chapter 4 explains the performance reproducibility of OSCs, involving both unrubbed and rubbed devices where their PV performance parameters are compared side-by-side. Additionally, the compositional, morphological and structural studies

are carried out to investigate the mechanism of the enhanced photovoltaic performance of the rubbed OSCs. This chapter also provides the detailed evaluation on the individual impact of rubbing and annealing on the enhanced PV performance of BL OSCs. In this regards, the compositional and structural characterizations of the active layers are mostly correlated with the PV performance of OSCs.

Lastly, Chapter 5 summarizes the findings throughout this research work and proposes the related plans that can be possibly carried out in the future.

1.10 References

1) A. Mohammad Bagher, Am. J. Opt. Photonics **3**, 94 (2015).
2) P.W.M. Blom, V.D. Mihailetchi, L.J.A. Koster, and D.E. Markov, Adv. Mater. **19**, 1551 (2007).
3) L. Dou, J. You, Z. Hong, Z. Xu, G. Li, R.A. Street, and Y. Yang, Adv. Mater. **25**, 6642 (2013).
4) S.S. Hegedus and W.N. Shafarman, Prog. Photovoltaics Res. Appl. **12**, 155 (2004).
5) S. Lizin, S. Van Passel, E. De Schepper, W. Maes, L. Lutsen, J. Manca, and D. Vanderzande, Energy Environ. Sci. **6**, 3136 (2013).
6) H. Ohkita and S. Ito, Polymer **52**, 4397 (2011).
7) B. Yin, Q. Liu, L. Yang, X. Wu, Z. Liu, Y. Hua, S. Yin, and Y. Chen, J. Nanosci. Nanotechnol. **10**, 1934 (2010).
8) Y.J. Jeon, S. Lee, R. Kang, J.E. Kim, J.S. Yeo, S.H. Lee, S.S. Kim, J.M. Yun, and D.Y. Kim, Sci. Rep. **4**, 6953 (2014).
9) S. Li, L. Ye, W. Zhao, S. Zhang, S. Mukherjee, H. Ade, and J. Hou, Adv. Mater. **28**, 9423 (2016).
10) H. Bin, L. Gao, Z.G. Zhang, Y. Yang, Y. Zhang, C. Zhang, S. Chen, L. Xue, C. Yang, M. Xiao, and Y. Li, Nat. Commun. **7**, 1 (2016).
11) I. Etxebarria, J. Ajuria, and R. Pacios, J. Photonics Energy **5**, 057214 (2015).
12) Z. He, B. Xiao, F. Liu, H. Wu, Y. Yang, S. Xiao, C. Wang, T.P. Russell, and Y. Cao, Nat. Photonics **9**, 174 (2015).
13) T. Ameri, N. Li, and C.J. Brabec, Energy Environ. Sci. **6**, 2390 (2013).
14) Q. Ma, Z. Jia, L. Meng, J. Zhang, H. Zhang, W. Huang, J. Yuan, F. Gao, Y. Wan, Z. Zhang, and Y. Li, Nano Energy **78**, 105272 (2020).
15) Z. Liu, J. Park, B. Li, H.P. Chan, D.K. Yi, and E.C. Lee, Org. Electron. **84**, 105802 (2020).

16) nrel.gov/pv/assets/pdfs/best-research-cell-efficiencies.20200925.pdf

17) H. Huang and J. Huang, Organic and Hybrid Solar Cells (Springer International Publishing, New York, 2014), pp. 1-274.

18) T. Xu and L. Yu, Mater. Today **17**, 11 (2014).

19) C.J. Brabec, N.S. Sariciftci, and J.C. Hummelen, Adv. Funct. Mater. **11**, 15 (2001).

20) V. Vohra, B. Dörling, K. Higashimine, and H. Murata, Appl. Phys. Express **9**, 1 (2016).

21) V. Vohra, G. Arrighetti, L. Barba, K. Higashimine, W. Porzio, and H. Murata, J. Phys. Chem. Lett. **3**, 1820 (2012).

22) J. Hou and X. Guo, in Org. Sol. Cells, edited by W.C.H. Choy (Springer-Verlag London, 2013), pp. 17–42.

23) D. Kajiya, S. Ozawa, T. Koganezawa, and K.I. Saitow, J. Phys. Chem. C **119**, 7987 (2015).

24) J.C. Bernède, J. Chil. Chem. Soc. **53**, 1549 (2008).

25) V. Jain, B.K. Rajbongshi, A. Tej Mallajosyula, G. Bhattacharjya, S.S. Kumar Iyer, and G. Ramanathan, Sol. Energy Mater. Sol. Cells **92**, 1043 (2008).

26) Y. Jang, J.W. Seo, J. Seok, J.Y. Lee, and K. Kim, Polymers. **7**, 1497 (2015).

27) A.L. Ayzner, C.J. Tassone, S.H. Tolbert, and B.J. Schwartz, J. Physc. Chem. C **113**, 20050 (2009).

28) J. Seok, T.J. Shin, S. Park, C. Cho, J.-Y. Lee, D. Yeol Ryu, M.H. Kim, and K. Kim, Sci. Rep. **5**, 8373 (2015).

29) J. Huang, J.H. Carpenter, C.Z. Li, J.S. Yu, H. Ade, and A.K.Y. Jen, Adv. Mater. **28**, 967 (2016).

30) V. Vohra, M. Campoy-Quiles, M. Garriga, and H. Murata, J. Mater. Chem. **22**, 20017 (2012).

31) L. Benatto, C.F.N. Marchiori, T. Talka, M. Aramini, N.A.D. Yamamoto, S. Huotari, L.S. Roman, and M. Koehle, Thin Solid Films **697**, 137827 (2020).

32) J.J. Rubio Arias and M. de F. Vieira Marques, React. Funct. Polym. **113**, 58 (2017).

33) G. Li, V. Shrotriya, J. Huang, Y. Yao, T. Moriarty, K. Emery, and Y. Yang, Nat. Mater. **4**, 864 (2005).

34) J.H. Lee, M. Takafuji, T. Sagawa, and H. Ihara, Sol. Energy Mater. Sol. Cells **147**, 68 (2016).

35) Z. Li, X. Xu, W. Zhang, W. Ma, A. Yartsev, O. Inganäs, M.R. Andersson, R.A.J. Janssen, and E. Wang, J. Am. Chem. Soc. **138**, 10935 (2016).

36) V. Vohra, O. Notoya, T. Huang, M. Yamaguchi, and H. Murata, Polymer **55**, 2213 (2014).

37) N. Espinosa and F.C. Krebs, Sol. Energy Mater. Sol. Cells **120**, 692 (2014).

38) M.B. Salim, R. Nekovei, and R. Jeyakumar, Sol. Energy 198, 160 (2020).

39) T. Ameri, P. Khoram, J. Min, and C.J. Brabec, Adv. Mater. **25**, 4245 (2013).

40) B.A. Gregg, J. Phys. Chem. B **107**, 4688 (2003).

41) K.A. Mazzio and C.K. Luscombe, Chem. Soc. Rev. 44, 78 (2014).

42) I. Arbouch, Y. Karzazi, and B. Hammouti, Phys. Chem. News **72**, (2014).

43) Q. An, F. Zhang, J. Zhang, W. Tang, Z. Deng, and B. Hu, Energy Environ. Sci. **9**, 281 (2015).

44) Z. Zhu, D. Mühlbacher, M. Morana, M. Koppe, M.C. Scharber, D. Waller, G. Dennler, and C.J. Brabec, in High-Efficient Low-Cost Photovoltaics Recent Dev., edited by V. Petrova-Koch, R. Hezel, and A. Goetzberger (Springer-Verlag, Heidelberg, 2009), pp. 195–222.S.

45) Nagamatsu, W. Takashima, K. Kaneto, Y. Yoshida, N. Tanigaki, K. Yase, and K. Omote, Macromolecules **36**, 5252 (2003).

46) T. Anzai, W. Porzio, and V. Vohra, J. Chem. **2017**, 1 (2017).

47) M. Aryal, K., K. Trivedi, and W. Hu, ACS Nano **3**, 3085 (2009).

48) L. Hartmann, K. Tremel, S. Uttiya, E. Crossland, S. Ludwigs, N. Kayunkid, C. Vergnat, and M. Brinkmann, Adv. Funct. Mater. **21**, 4047 (2011).

49) V. Vohra, W. Mróz, S. Inaba, W. Porzio, U. Giovanella, and F. Galeotti, ACS Appl. Mater. Interfaces **9**, 25434 (2017).

50) N. Espinosa, R. García-Valverde, A. Urbina, and F.C. Krebs, Sol. Energy Mater. Sol. Cells **95**, 1293 (2011).

51) O.P.M. Gaudin, I.D.W. Samuel, S. Amriou, and P.L. Burn, Appl. Phys. Lett. **96**, 3 (2010).

52) S. Sankaran, K. Glaser, S. Gärtner, T. Rödlmeier, K. Sudau, G. Hernandez-Sosa, and A. Colsmann, Org. Electron. Physics, Mater. Appl. **28**, 118 (2016).

53) R.R. Søndergaard, M. Hösel, and F.C. Krebs, J. Polym. Sci. Part B Polym. Phys. **51**, 16 (2013).

54) V. Vohra, K. Higashimine, T. Murakami, and H. Murata, Appl. Phys. Lett. **101**, 173301 (2012).

55) P. Cheng, C. Yan, Y. Wu, S. Dai, W. Ma, and X. Zhan, J. Mater. Chem. C 4, 8086 (2016).

56) E.L. Lim, C.C. Yap, M.A. Mat Teridi, C.H. Teh, A.R. Bin Mohd Yusoff, and M.H. Hj Jumali, Org. Electron. Physics, Mater. Appl. **36**, 12 (2016).

Chapter 2

OPTIMIZATION OF BILAYER P3HT/PCBM OSCs AND CHARACTERIZATIONS OF P3HT FILMS

2.1 Introduction

2.1.1 Bilayer P3HT/PCBM OSCs

The bilayer OSCs are regarded as the model of operational OSCs having donor-acceptor components. The functional OSCs consist of donor/acceptor active layer sandwiched between the metal and transparent electrodes. The basic BL OSCs consist of at least a transport layer, typically a hole transport layer in regular architecture. Poly(3,4-ethylenedioxythiophene)-poly(styrenesulfonate) (PEDOT:PSS) has been a well-known hole transport layer which is usually inserted between a transparent electrode [e.g. indium tin oxide (ITO)] and a metal electrode. Its functions are to smoothen the rough ITO surface and provide favorable energy level alignment with the donor polymer as shown in Figure 2.1a.[1] This buffer layer is made up of a thiophene-based conjugated polymer and sulfonated polystyrene. These components carry positive and negative charges respectively, thus it has good conductivity.[2] Besides, it has good transparency and high work function of ca. 5.2 eV.[3] The high work function reduces the barrier height between anode and polymer interface improving the hole transport from polymer to anode. Additionally, this transport layer prevents the charge recombination in the active layer through its electron blocking property.[2]

Beside the buffer layer, the properties of active layer play an important role in governing the operation mechanism OSCs. These properties can be examined through morphological, optical and structural studies. The thorough understanding of these properties will help to appropriately alter the active layer to realize the device with decent performance. Among the

donor materials for OSCs, P3HT has been a well-known material that represents the use of conjugated polymer as the donor layer. It has been widely investigated as it possesses favorable absorption spectrum within the wavelength region of visible light. Besides, it has the flexibility of solvent choice as it can be easily dissolved in various solvents including chloroform (CF), chlorobenzene (CB) and 1,2-dichlorobenzene.[4,5] Also, it comes with a range of properties such as the regioregularity (RR), molecular weight (M_w) and polydispersity index (PDI). The selection of its properties is often based on the desired features of P3HT film including its morphology, crystallinity, absorbance and molecular orientation.

On the other hand, PCBM is a buckminsterfullerene derivative that has been widely used as a standard electron accepting material for OSCs.[6] Most of the high performance solar cells have been fabricated using either $PC_{61}BM$ or $PC_{71}BM$.[6] $PC_{61}BM$ is more commonly employed as the acceptor layer rather than $PC_{71}BM$ as it contributes to stable and reproducible devices.[7] As PCBM is highly soluble in the common solvents, the P3HT/PCBM bilayer device uses a bottom P3HT layer with relatively poor solubility in PCBM solvent.[8] This attribute ensures that the upper PCBM layer penetrates at a certain degree into P3HT layer.

Apart from the film properties, the experimental and device fabrication procedures need to be carefully considered to enhance the P3HT/PCBM device performance. One of the common approaches is the thermal annealing of the OSCs. Thermal annealing has been a well-known approach that is capable to affect the properties of active layer through the reorganization, aggregation and further crystallization within the initially amorphous or poorly crystalline as-deposited active layer to form the larger well-organized domains.[9,10] These advantages were reported to significantly enhance the OSCs.[11]

At the beginning of sample preparation, P3HT solution will be prepared from the P3HT powder with chlorobenzene solvent to prepare P3HT films. The properties of individual P3HT films are expected to influence the performance of the fabricated bilayer OSCs having donor/acceptor components (Fig. 2.1b).

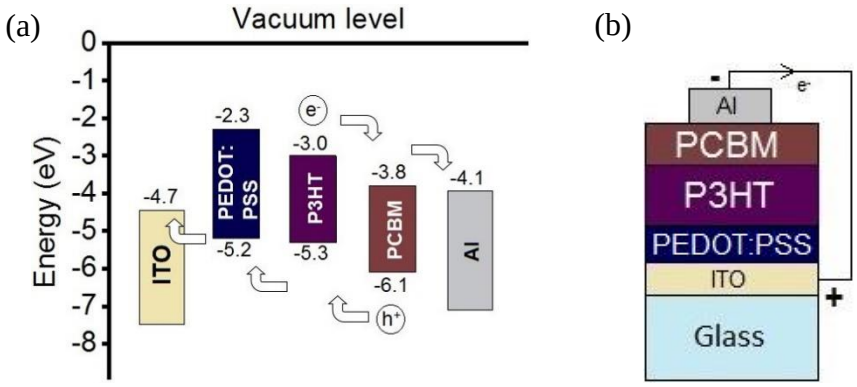

Figure 2.1 (a) Energy levels[3] and (b) schematic diagram of bilayer P3HT/PCBM OSCs.

2.1.2 The State-of-the-art of the Performance of Bilayer P3HT/PCBM OSCs

Single layer OSCs was reported to exhibit poor device performance (< 0.1% *PCE*) as the electric field resulting from the difference between the two electrodes is insufficient to split the excitons.[12] Since the finding of operational OSCs via single layer architecture, a few promising device geometries of OSCs emerged as a result of research and development in organic and optoelectronics field. The bilayer device architecture has been the essential device geometry as it features a significant enhancement of device performance exceeding 1% *PCE*.[13] P3HT and PCBM have been commonly used as the conjugated polymer and fullerene derivative for the donor and acceptor layers in OSCs. The use of P3HT and PCBM to fabricate the OSCs in BL architecture was reported to exhibit *PCE* of ca. 3.5% thanks to the control of sequential deposition via orthogonal solvents.[14] With the aid of rubbing process on P3HT layer, the BL P3HT/PCBM has achieved the maximum power conversion efficiency of 3.99% which is comparable to that of regular BHJ P3HT:PCBM device.[15] The continuous effort to improve the performance of bilayer P3HT/PCBM device is possible by optimizing the device fabrication procedures in view to overcome the current state-of-the-art OSCs. For example, by taking advantage of BL architecture, the morphology and donor-acceptor concentration

gradient at P3HT/PCBM interface can be controlled by varying the polymer solvent and introducing the annealing heat treatment.

2.2 Experimental Procedure

2.2.1 Fabrication and PV Evaluation of Bilayer P3HT/acceptor OSCs and P3HT Film Samples

The fabrication procedures of BL OPV devices involves several steps where the standard procedures follow the reported experimental procedures to fabricate the bilayer P3HT/acceptor OPV device.[5,15] The steps which are not found in the reported paper (e.g. stirring conditions of P3HT solution) are based on the guidance taught in the laboratory. Basically, device fabrication procedures involve the substrate cleaning, deposition of active layers, deposition of metal electrode, device encapsulation and heat treatment. An ITO-coated glass substrate is used to fabricate the device while a quartz or double-sided polished Si wafer is used in place of ITO-coated glass substrate to fabricate the sample. Initially, the ITO-coated glass substrates were ultrasonically cleaned in acetone, Semico clean (detergent), pure water and isopropyl alcohol cleaning solvents. They are cleaned within low and high frequency range (28, 45 and 100 kHz alternately). To remove the organic impurities, they were subjected to UV/ozone treatment for 30 min. PEDOT:PSS (Heraeus, Clevious P VP AI 4083) was spin coated on the cleaned substrates at 4000 rpm for 30 s. The active layer solution preparation and spin coating were carried out inside the nitrogen-filled glove box. P3HT powder (BASF Sepiolid P200, >98% RR, M_w: 20-30 kDA, PDI: 2.0) was dissolved in CB to prepare 30 mg/mL P3HT solution. This solution was stirred at 200 rpm for ca. 3 hr at 50 °C. Then the spin coating of P3HT solution was performed at 2500 rpm for 30 s.

The acceptor solution was prepared by dissolving the acceptor material using an organic solvent. Usually, the acceptor that easily dissolves in its solvent does not require the additional stirring process. The acceptor solution was spin coated on top of donor layer. To prepare the

PCBM top layer, the PCBM powder (Luminescence Technology) was dissolved in dichloromethane (DCM) solvent to obtain 10 mg/mL PCBM solution. After that, the PCBM solution was spin coated on P3HT layer at 4000 rpm for 10 s. The inert atmosphere (nitrogen-filled with <1% oxygen concentration) was retained from the preparation P3HT solution until the acceptor spin coating. To complete the device, the metal electrode was evaporated on top of the active layer at a proper evaporation rate. Using a vacuum evaporator, aluminum (Al) electrode was deposited at ca. 7 Å/s evaporation rate. This electrode evaporation was performed through a patterned mask that defines the individual cell area. The Al is evaporated on the active layer at 4 mm^2 evaporation mask to realize the metal electrode with 100 nm thick.

The final step is the device encapsulation process in which the glass slide was used to protect the active layer from the oxygen and moisture. The encapsulation process was carried out after the Al evaporation in which the device is covered with a glass slide to protect the active layer from the oxygen and moisture. The overall device fabrication procedures are shown in Fig. 2.2.

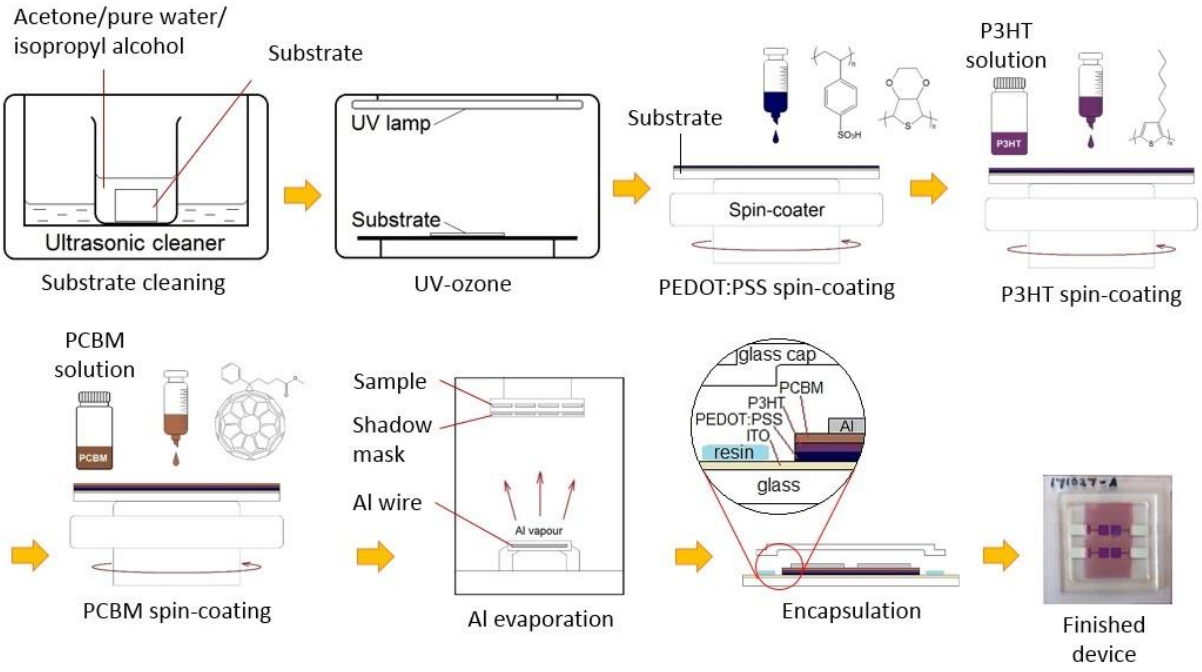

Figure 2.2 Fabrication procedures of bilayer P3HT/PCBM OSCs.

The fabricated device has four cells each with 4 mm^2 area as in Figure 2.3. The fabricated devices and samples were firstly characterized in ADP condition. Then, the similar characterizations were repeated on the annealed devices (140 °C, 10 min). The photovoltaic performance of the P3HT/PCBM OSCs is measured using Keithley 2400 Sourcemeter paired with the solar simulator under 1 sun (AM1.5G, 100 mW cm^{-2}) irradiation.

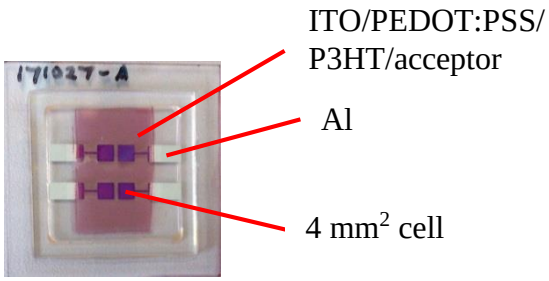

Figure 2.3. The image of bilayer P3HT/PC_{61}BM OSCs.

2.2.2 Optimization Process of OSCs Fabrication Parameters: Substrate Cleaning, Electron Acceptor, P3HT Solvent, Heat Treatment and Evaporation Rate of Al Electrode

The properties of active layer play important roles in governing the performance of bilayer P3HT/PCBM OSCs. There are several approaches that can be applied to adjust the properties of active layer. Depending upon the desired properties of active layer, the experimental procedures would be varied. Apart from the varied procedures, the other procedures were keep consistent as described in Section 2.2.1.

The presence of the impurities in the active layer might degrade the device performance. This could be confirmed by comparing the device performance of cleaned and non-cleaned substrate. To do so, one substrate was ultrasonically cleaned while another substrate was used as-received without cleaning process.

On the other hand, the type of solvent used to dissolve the donor material affects the properties of deposited film because each solvent has its own boiling point. The evaporation

rate of the solvent that has low boiling point is high and would result in higher degree of organization in the polymer structure.[16,17] CB and CF having boiling points of 132 and 61 °C respectively,[17] were used to observe the effect of solvent evaporation rate on the device performance. P3HT was dissolved in CB and CF separately to prepare 30 mg/mL P3HT solutions.

The use of different acceptors could influence the device performance as well. Five different fullerene-based acceptors which are [6,6]-phenyl-C_{61}-butyric acid methyl ester ($PC_{61}BM$), [6,6]-phenyl-C_{71}-butyric acid methyl ester ($PC_{71}BM$), *N*-phenyl[60]fulleropyrrolidines derivatives (HNP and PNP) and YY03009 were used. Each acceptor was dissolved in DCM to obtain 10 mg/mL solutions. These acceptor solutions were spin-coated on P3HT layers at 4000 rpm for 10 s.

The evaporation rate of metal electrode was said to affect its grain size and surface roughness.[18] In this regard, the formation of metal electrode would indirectly influence the interface between the metal electrode and the underlying active layer. Using the vacuum evaporator, 100 nm thick Al electrode was deposited at average evaporation rates of ca. 3 and 7 Å/s.

Thermal annealing is performed by heating the substrates to temperatures greater than the glass transition temperature of the donor material.[11] This allows the donor film to crystallize and reorganize the aggregates of acceptor film.[19] Thermal annealing can be classified as pre-annealing and post-annealing. Pre-annealing is usually performed before evaporating the metal electrode. It was followed by the evaporation of a thin electron transport layer made up of calcium (Ca) or lithium fluoride (LiF). On the other hand, post-annealing involves the heat treat treatment after electrode evaporation typically on encapsulated device. To investigate the effect of pre-annealing and post-annealing on the device performance, the P3HT/PCBM devices were pre-annealed and post-annealed at 140 °C for 10 min.

2.2.3 Characterizations of P3HT Film Samples

For the P3HT film samples, only P3HT solution was spin coated on quartz substrates or double-sided polished Si wafer and there is no further steps done. The thickness and surface roughness of P3HT films were measured using Keyence VN-8000 Atomic Force Microscope (AFM). The image scanning range was set to $5\mu m^2$. The absorption spectra of P3HT film were measured using Jasco V570 UV-visible Spectrophotometer. The measurement was performed within 400-800 nm visible light region. The evaluation of molecular orientation in P3HT films were performed via p-polarized multiple-angle incidence resolution spectrometry (pMAIRS) technique using Thermo Fisher Scientific Nicolet 6700 Fourier-transform infrared spectroscopy (FTIR) equipped with an automatic pMAIRS equipment. For pMAIRS measurement, P3HT films were deposited on the double-sided polished silicon wafers. The morphological, optical and structural properties of ADP and AND P3HT films acquired through these characterizations provide the understanding on the reasons behind the performance of P3HT/PCBM devices before and after annealing.

2.3 Results and Discussion

2.3.1 Effect of Substrate Cleaning on Photovoltaic Performance of P3HT/PCBM Devices

The impurities were said to reduce the mobility, reducing the charge transport efficiency within the impure region.[20] The dust and dirt on the surface of the substrates can lead to the formation of undesirable defects during the device fabrication. Usually, the substrates are thoroughly cleaned to remove the dust and dirt from their surface before proceeding to the device fabrication.

The effect of substrate cleaning on the photovoltaic performance of bilayer P3HT/PCBM OSCs can be observed on the *J-V* curves in Figure 2.4. It can be seen that there is almost no

change in the *J-V* curves of ADP devices regardless of substrate cleaning condition. The clearer comparison of the device performance is shown in Table 2.1 and Figure 2.5. The cleaned device shows slightly higher J_{sc} and *FF* compared to non-cleaned device. Regardless the cleaning condition, the devices possess equivalent V_{oc}. The resultant *PCE* of the ADP devices is almost the same. The non-cleaned and cleaned ADP devices have *PCE* of 1.70% and 1.75% respectively.

The significant improvement on PV performance can be seen on the AND devices where the cleaned device outperformed the non-cleaned device. Post-annealing results in significant increments of J_{sc}, V_{oc} and *FF* in the cleaned device, contributing to its substantially higher *PCE* (2.94%) in comparison to that of non-cleaned AND device (2.26%). The slightly lower PV performance of the non-cleaned devices could be attributed to the presence of the impurities around PEDOT:PSS/ITO interface. The annealing was reported to induce the crystallization of active layer that enhances the transport of dissociated charges to electrodes. The presence of impurities near to ITO may disturb collection of dissociated holes at ITO electrode.

It can be seen through this experiment that the cleaning process is necessary to fabricate the bilayer P3HT/PCBM OPV device with the decent PV performance.

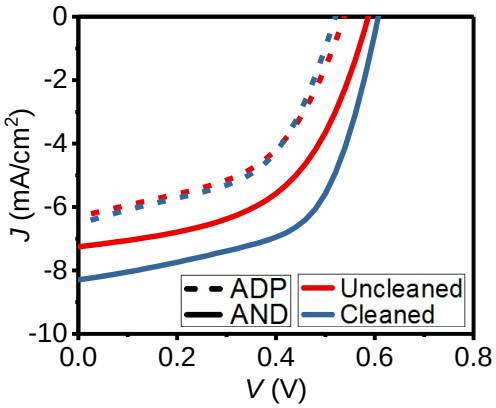

Figure 2.4. *J-V* curves of bilayer P3HT/PC_{61}BM OSCs with respect to different substrate cleaning conditions.

Table 2.1. PV characteristics of bilayer P3HT/PCBM OSCs corresponding to different substrate cleaning conditions.

Substrate cleaning	J_{sc} (mA/cm^2)		V_{oc} (V)		*FF*		*PCE* (%)	
	ADP	AND	ADP	AND	ADP	AND	ADP	AND
Uncleaned	6.27	7.25	0.54	0.59	0.50	0.53	1.70	2.26
Cleaned	6.48	8.28	0.52	0.61	0.52	0.59	1.75	2.94

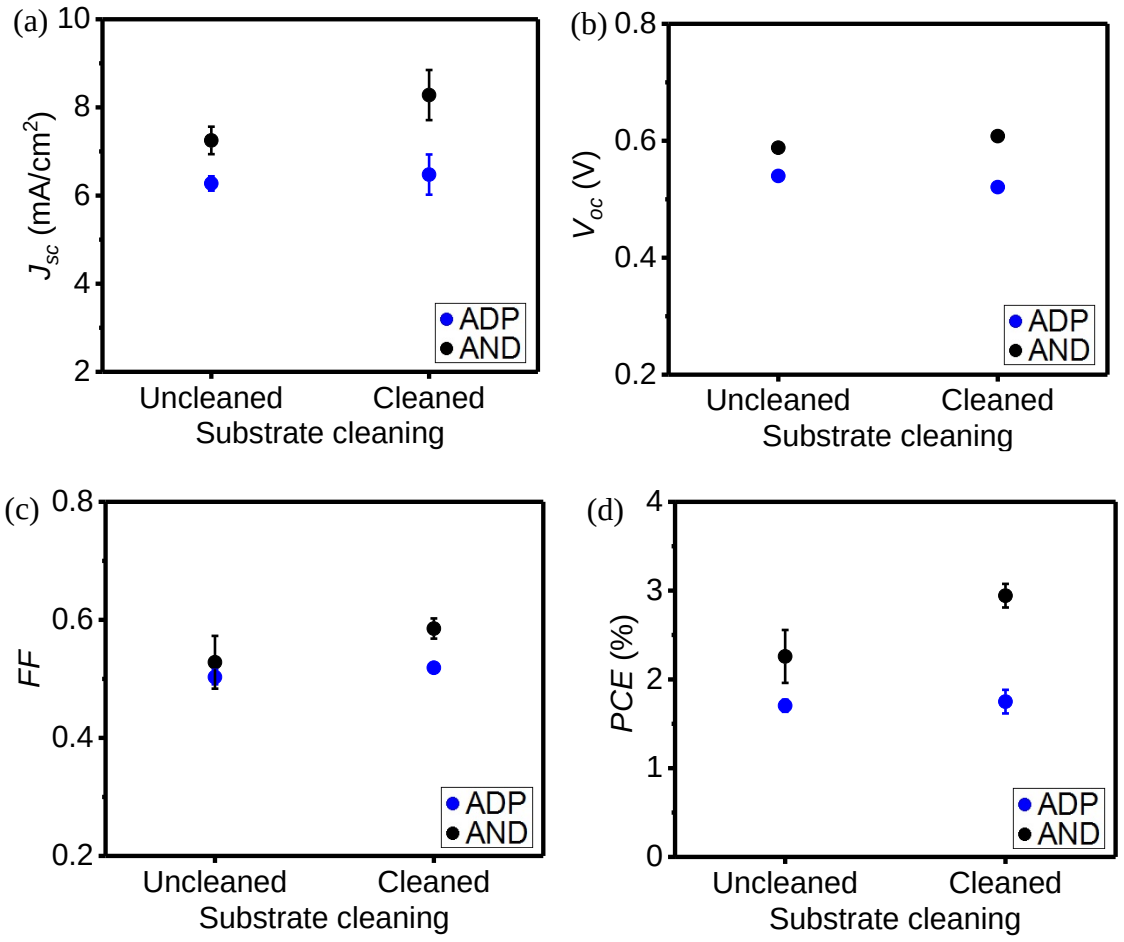

Figure 2.5. Photovoltaic performance of bilayer P3HT/$PC_{61}BM$ OSCs: (a) J_{sc}, (b) V_{oc}, (c) *FF* and (d) *PCE* corresponding to different substrate cleaning conditions.

2.3.2 Effect of Different P3HT Solvents on Photovoltaic Performance of P3HT/PCBM OSCs

P3HT powders are soluble in certain organic solvents such as CF, CB and toluene. Also, they are known to be partially soluble in tetrahydrofuran (THF) and diethyl ether (Et_2O). Through solution process, the thickness of P3HT film can be controlled based on the evaporation rate or boiling point (bp) of its solvent. For example, CF-dissolved P3HT results in thicker P3HT film compared to CF-dissolved P3HT because CF has higher evaporation rate (lower bp) than CB. In other words, the evaporation rate of organic solvent governs the crystal growth of P3HT layer affecting its thickness.

As shown in the *J-V* curves shown in Fig. 2.6, the ADP CF-dissolved device exhibits very high V_{oc}, which is almost one-fold higher than that of CB-dissolved device. Both ADP devices have almost the smilar J_{sc} which is around 5 mA/cm^2. Table 2.2 specifies each PV characteristic while Fig. 2.7 compares the PV parameters of the devices. It can be seen that the CF-dissolved device have slightly higher J_{sc} compared to CB-device. This is due to the slightly thicker CF-dissolved P3HT film that absorbs more light. The thicker P3HT film is attributed to the high evaporation rate of CF solvent. The low charge recombination in thicker CF-dissolved active layer causes relatively large V_{oc} in CF-dissolved device. The rapid crystal growth of the CF-dissolved P3HT results in its poor crystallinity. The poor crystalline active layer restricts the mobility of the dissociated, thus significantly reducing the *FF* in CF-dissolved device.

By looking at the *J-V* curves, the post-annealing process results in relatively low increment of V_{oc} in CF-dissolved device. The crystallization of active layer further improves the crystallinity of CB-dissolved layer. Therefore, the charge transport in the AND CB-dissolved layer is more efficient with the reduced chance of charge recombination. This explain the reason behind the larger increment of V_{oc} in CB-dissolved device. The increment of J_{sc} is comparable in CB-dissolved and CF-dissolved devices. Regardless the annealing condition, the J_{sc} in CF-dissolved devices is always greater than that of CB-dissolved devices because of

the higher light absorption into thicker CF-dissolved P3HT films. The *FF* of CF-dissolved device could not surpass that of CB-dissolved device because the annealing of poorly crystalline CF-dissolved P3HT film does not result in the film with higher crystallinity than the AND CB-dissolved film. The low evaporation rate of CB results in slow P3HT crystal growth, thus high crystalline ADP film which is further crystallized by annealing.

The influence of CB and CF solvents on PV characteristics bring about the *PCE* of 1.37% and 0.68% in ADP CB-dissolved and CF-dissolved devices respectively. The corresponding annealed CB-dissolved and CF-dissolved devices exhibit the increments of *PCE* being 2.25% and 2.08%. It can be pointed out that the selection of appropriate solvent is essential to get the device with good performance. Evaporation rate is a good trait that can be used to appropriately select the solvent to dissolve the P3HT.

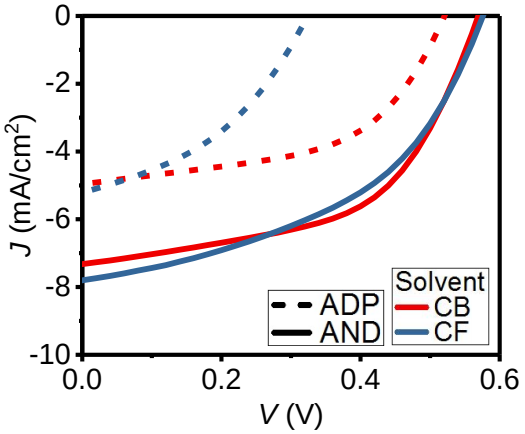

Figure 2.6. *J-V* curves of bilayer P3HT/$PC_{61}BM$ OSCs with respect to different solvents of P3HT.

Table 2.2. PV characteristics of bilayer P3HT-based OSCs corresponding different solvents of P3HT.

P3HT solvent	J_{sc} (mA/cm^2)		V_{oc} (V)		*FF*		*PCE* (%)	
	ADP	AND	ADP	AND	ADP	AND	ADP	AND
CB	4.94	7.32	0.52	0.57	0.53	0.54	1.37	2.25
CF	5.18	7.71	0.30	0.57	0.40	0.46	0.68	2.08

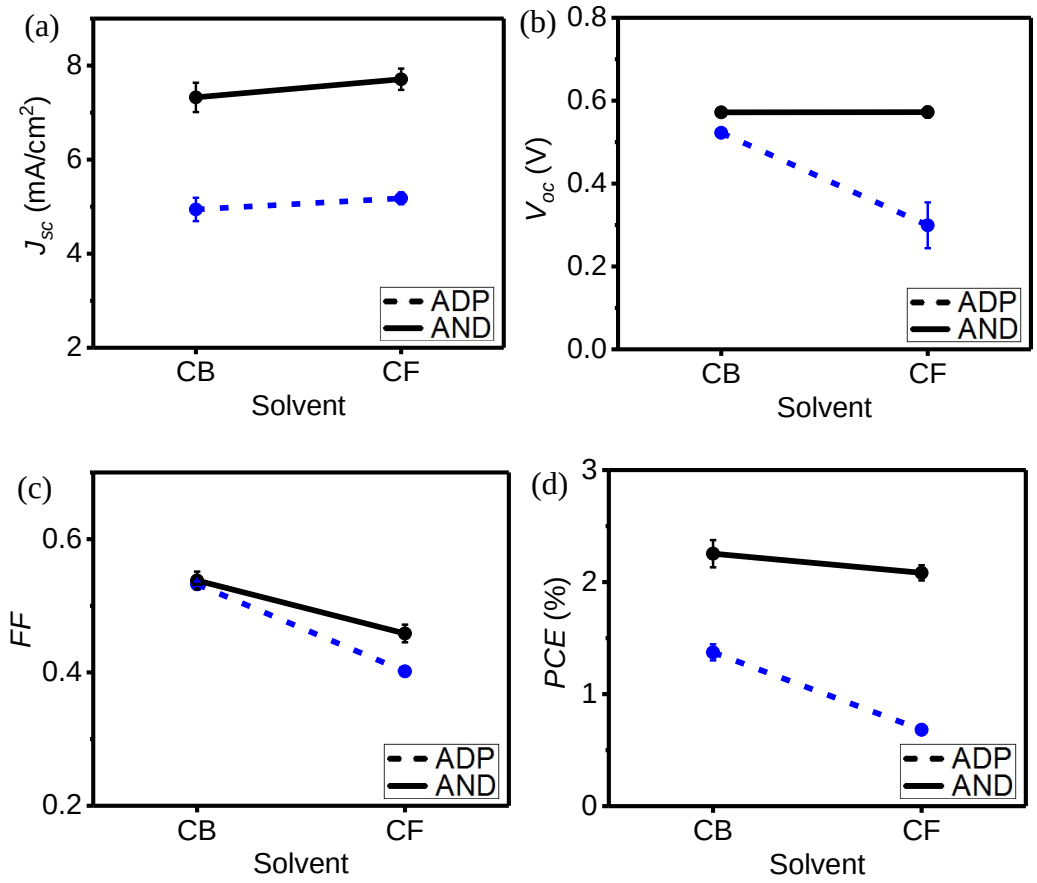

Figure 2.7. Photovoltaic performance of bilayer P3HT/$PC_{61}BM$ OSCs: (a) J_{sc}, (b) V_{oc}, (c) *FF* and (d) *PCE* corresponding to different solvents of P3HT.

2.3.3 Effect of Different Electron Acceptors on Photovoltaic Performance of Bilayer P3HT-based OSCs

The fullerene-based electron acceptor is typically made up of at least a fullerene derivative component. It was said that the limiting factor of electron acceptor that limits the electron collection is its low mobility. This factor is related to the crystallinity of the acceptor layer. Low crystalline acceptor will result in low device performance due to high charge recombination. Charge recombination reduces V_{oc} and *FF* that governs the power conversion of the device.

The *J-V* curves in Fig. 2.8 indicates the distinctive performance of the P3HT-based bilayer OPV devices corresponding to different acceptors. In case of ADP devices, $PC_{61}BM$ results in

the highest J_{sc}, followed by $PC_{71}BM$, HNP, PNP and YY03009. The devices with the new HNP and PNP acceptors exhibit top two highest V_{oc}. Note that the variation of J_{sc} is larger than that of V_{oc}. Table 2.3 and Fig. 2.9 compare the PV characteristics of each device with respect to different acceptors. The device with $PC_{61}BM$ shows the highest *FF* owing to its decent J_{sc} and V_{oc}. Therefore, this particular device has the highest *PCE* among the ADP devices.

Annealing is associated with the crystallization of the active layer that further enhances the OPV devices. The AND P3HT/$PC_{61}BM$ device outperforms the other devices due to its superior J_{sc} and *FF*. The device with YY03009 exhibits the largest increments of V_{oc} and *FF*. At particular solution preparation conditions (DCM solvent and 10 mg/mL concentration), $PC_{61}BM$ is implicitly regarded as the best acceptor possibly due to its optimal crystallinity. Its high crystallinity is shown by the highest J_{sc} and *FF* in P3HT/PCBM OSCs. The crystalline active layer absorbs more photon and thereby increases the J_{sc}. Also, the charges transport better in active layer with high crystallinity as reflected by high *FF* in P3HT/PCBM OSCs.

The variation of PV characteristics in the devices with different acceptors indicates the type of acceptor is a crucial factor that determines the performance of OSCs. The proper selection of acceptor with the optimal crystallinity will ensure the decent performance of the device particularly due to increase of J_{sc} and *FF*.

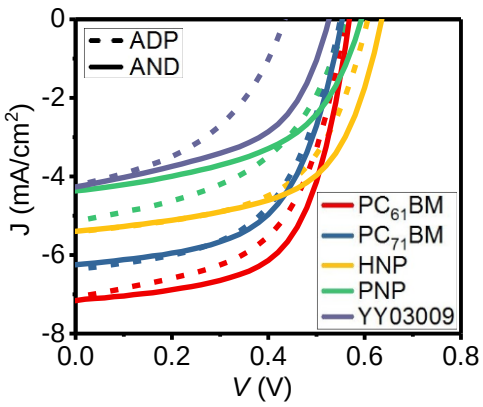

Figure 2.8. *J-V* curves of bilayer P3HT/$PC_{61}BM$ OSCs with respect to different electron acceptors.

Table 2.3. PV characteristics of bilayer P3HT-based OSCs corresponding to different electron acceptors.

Acceptor	J_{sc} (mA/cm^2)		V_{oc} (V)		*FF*		*PCE* (%)	
	ADP	AND	ADP	AND	ADP	AND	ADP	AND
$PC_{61}BM$	6.70	6.80	0.56	0.57	0.56	0.59	2.04	2.37
$PC_{71}BM$	6.43	6.36	0.55	0.55	0.53	0.56	1.87	1.97
HNP	5.28	5.17	0.61	0.64	0.51	0.57	1.57	1.89
PNP	4.87	4.18	0.57	0.59	0.49	0.50	1.34	1.22
YY03009	4.02	4.07	0.43	0.53	0.42	0.50	0.67	1.08

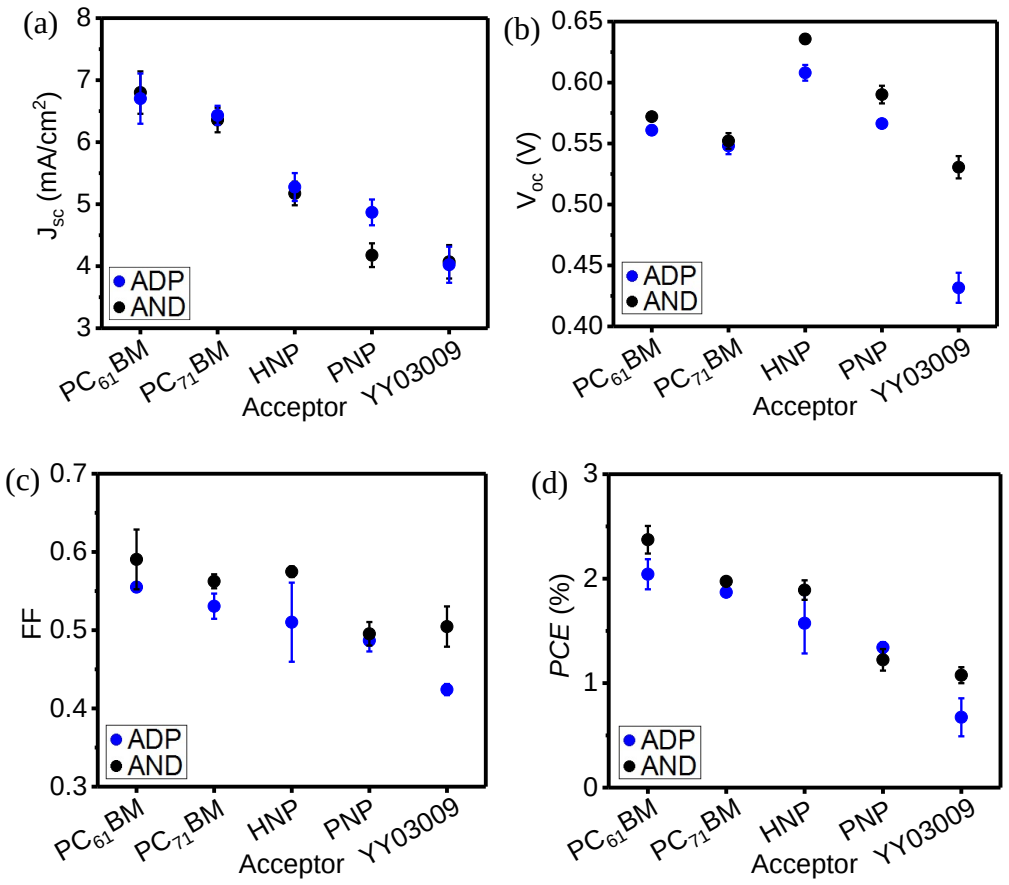

Figure 2.9. Photovoltaic performance of bilayer P3HT/$PC_{61}BM$ OSCs: (a) J_{sc}, (b) V_{oc}, (c) *FF* and (d) *PCE* corresponding to different electron acceptors.

2.3.4 Effect of Evaporation Rate of Al Electrode on Photovoltaic Performance of P3HT/PCBM OSCs

Al has been used as negative electrode for conventional BL device where the evaporation technique has been the method to deposit the Al on the active layer. During the fabrication of previous OPV devices, it was suspected that the Al evaporation possibly pre-annealed the active layer prior to encapsulation process. To validate such hypothesis, the effect of the evaporation rate on PV characteristics of typical bilayer P3HT/PCBM devices is investigated. The evaporation rate was set to two ranges which are 2-5 (average: 3 Å/s) and 5-10 Å/s (average: 7 Å/s).

The *J-V* curves in Fig. 2.10 show that the devices deposited with 3 and 7 Å/s have almost similar PV characteristics. Table 2.4 and Fig. 2.11 provide more details of the comparison of the device performance. The ADP devices exhibit similar V_{oc} and *FF*. The slightly higher J_{sc} results in the device with low Al evaporation rate (3 Å/s) results in its slightly better *PCE* (1%) compared to that with high Al evaporation rate (7 Å/s, 0.94% *PCE*).

The effective post-annealing of the devices with high Al evaporation rate contrasts with the assumption that the high Al evaporation rate would anneal the active layer. There are larger increments of each PV characteristic in the AND device with high Al evaporation rate. As a result, it has slightly better *PCE* (2.86%) than that with low Al evaporation rate (2.62%). It was reported in literature reviews that the grain size of Al electrode is dependent on its evaporation rate where the higher rate results in larger and rougher grain size.[18,21] In this manner, the (c)
rougher surface of Al deposited at 7 Å/s is provides higher surface area for more electron collection. This complies with the slightly higher *FF* in the device with high Al evaporation rate.

The effect of evaporation rate of Al electrode on the PV performance of BL P3HT/PC_{61}BM OSCs has been investigated. Comparing the devices with low and high Al evaporation rate, it

has been found that there is no much different between the high and low evaporation rate on device performance.

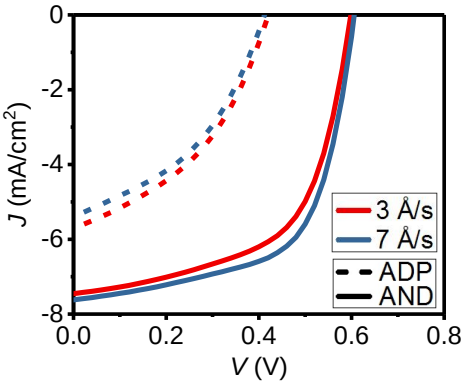

Figure 2.10. *J-V* curves of bilayer P3HT/$PC_{61}BM$ OSCs with respect to different evaporation rates of Al electrode.

Table 2.4 PV characteristics of bilayer P3HT/$PC_{61}BM$ OSCs corresponding to different evaporation rates of Al electrode.

Evaporation rate (Å/s)	J_{sc} (mA/cm^2)		V_{oc} (V)		*FF*		*PCE* (%)	
	ADP	AND	ADP	AND	ADP	AND	ADP	AND
3	5.69	7.46	0.42	0.60	0.42	0.58	1.00	2.62
7	5.40	7.63	0.42	0.60	0.42	0.62	0.94	2.86

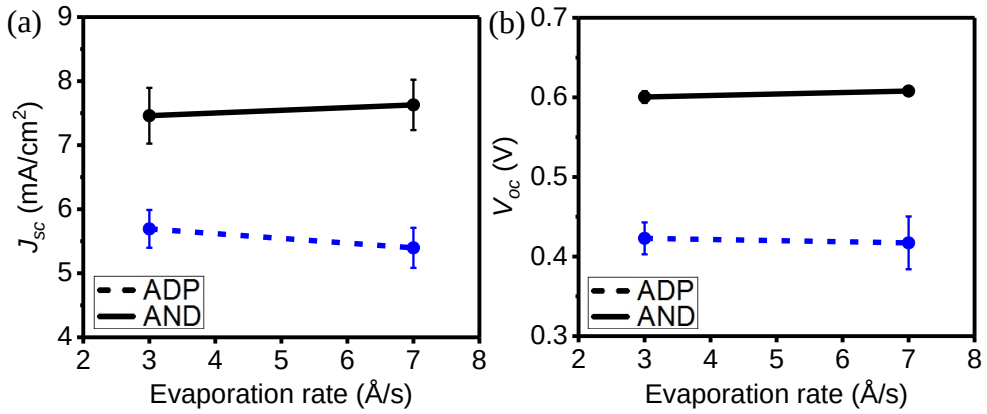

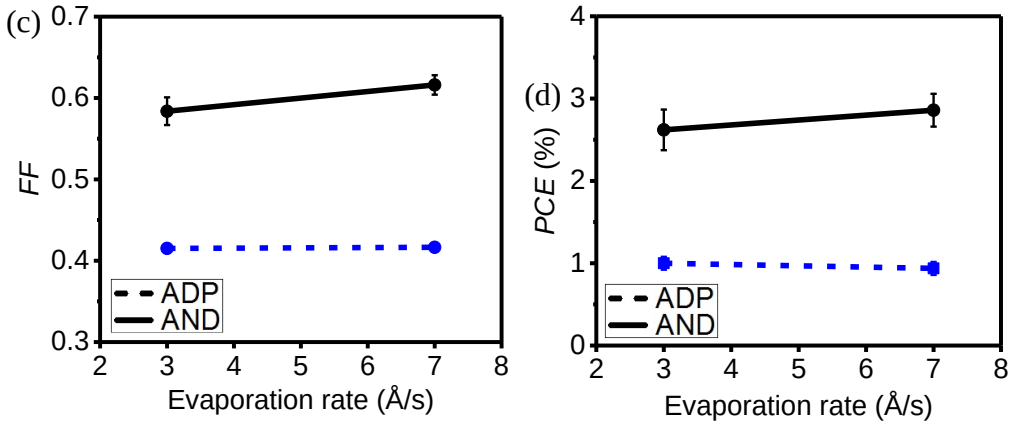

Figure 2.11. Photovoltaic performance of bilayer P3HT/$PC_{61}BM$ OSCs: (a) J_{sc}, (b) V_{oc}, (c) *FF* and (d) *PCE* corresponding to different evaporation rates of Al electrode.

2.3.5 Effect of Pre-annealing and Post-annealing on Photovoltaic Performance of P3HT/PCBM OSCs

The crystallization of active layer plays vital role in assisting the transport of holes and electrons after exciton dissociation at P3HT/PCBM interface. Annealing has been the viable heat treatment used to enhance the crystallization of active layer. The so-called pre-annealing is carried out prior to the deposition of metal electrode while the post-annealing is performed after depositing the metal electrode, typically once the device fabrication process is fully completed. The pre-annealing has been associated with the incorporation of thin LiF interlayer between the active layer and the Al electrode to impede the formation of craters during the Al evaporation.[22] To evaluate which annealing process results in better device performance, two P3HT/PCBM OSCs were fabricated. One device was pre-annealed while another device was post annealed at 140 °C for 10 min.

The PV performance evaluation is carried out by comparing the PV characteristic of AND devices. By looking at the *J-V* curves (Fig. 2.12), it can be found that the performance of pre-annealed (pre-AND) device is inferior to that of post-annealed (post-AND) device. The

quantitative comparison of the devices is shown by Table 2.5 and Fig. 2.13. Apart from the comparable *FF*, the apparently higher J_{sc} and V_{oc} in post-AND device result in its superior PCE (2.78%) compared to that of pre-AND device (2.53%).

It was found the post-annealing favors the superior performance of BL P3HT/PCBM device. Also, the use of LiF interlayer for this device is not necessary as shown by the undesirable performance of pre-AND device with the LiF.

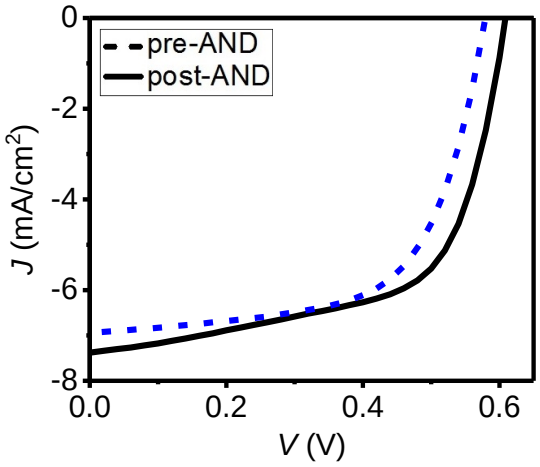

Figure 2.12. *J-V* curves of pre-annealed and post-annealed bilayer P3HT/$PC_{61}BM$ OSCs.

Table 2.5 PV characteristics of pre-annealed and post-annealed bilayer P3HT-based OSCs.

Heat treatment	J_{sc} (mA/cm^2)	V_{oc} (V)	*FF*	*PCE* (%)
Pre-annealing	6.94	0.58	0.63	2.53
Post-annealing	7.37	0.61	0.62	2.78

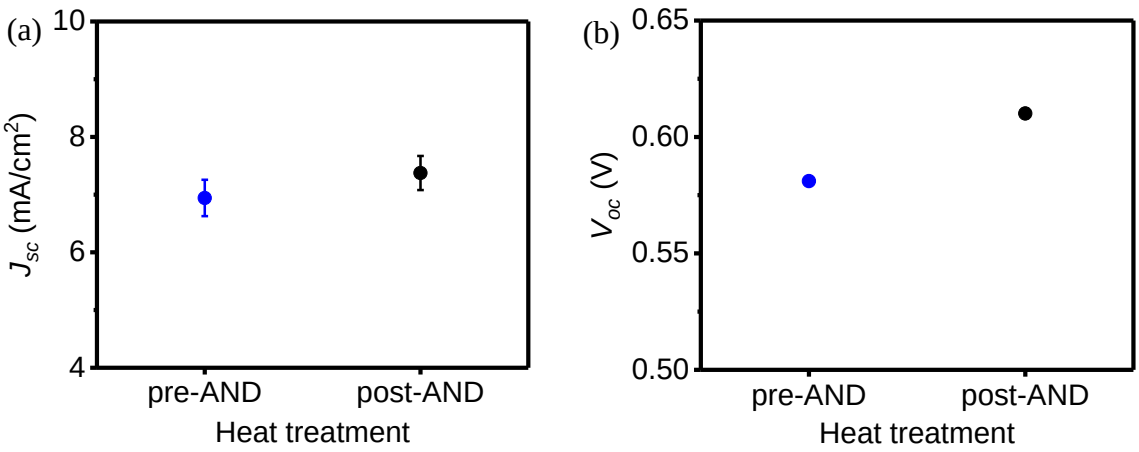

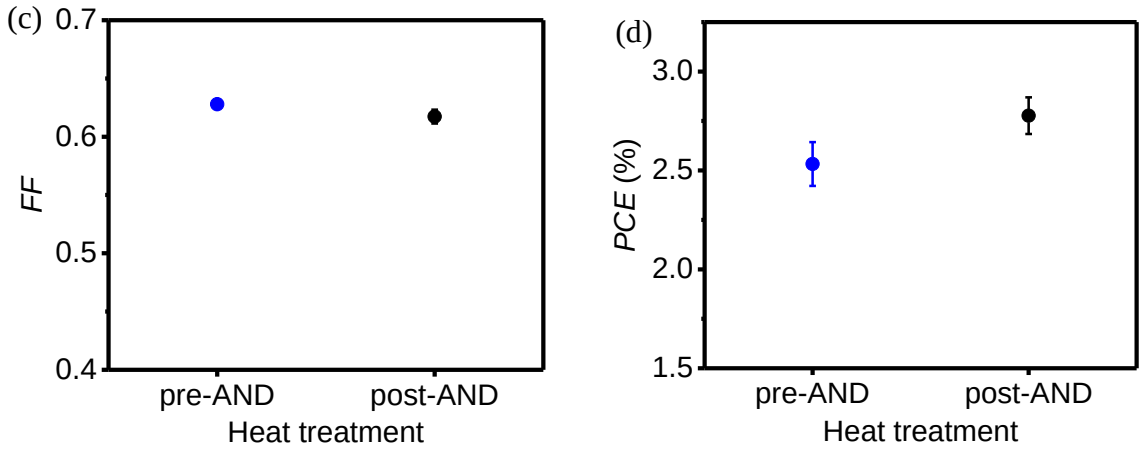

Figure 2.13. Photovoltaic performance of pre-annealed and post-annealed bilayer P3HT/$PC_{61}BM$ OSCs: (a) J_{sc}, (b) V_{oc}, (c) *FF* and (d) *PCE*.

2.3.6 Performance of Optimized Bilayer P3HT/PCBM OSCs

The optimized BL P3HT/PCBM OSCs were fabricated based on the optimized substrate cleaning, P3HT solvent, electron acceptor, Al electrode evaporation rate and heat treatment. The performance of ADP and AND BL OPV devices is represented by their *J-V* curves in Fig. 2.14 where the AND device significantly outperforms the ADP device as shown by its higher J_{sc} and V_{oc}. More square-shaped *J-V* curve of annealed device reflects that it has substantially higher *FF* due to the closer ratio between P_{max} and the product of J_{sc} and V_{oc}.[11,23]

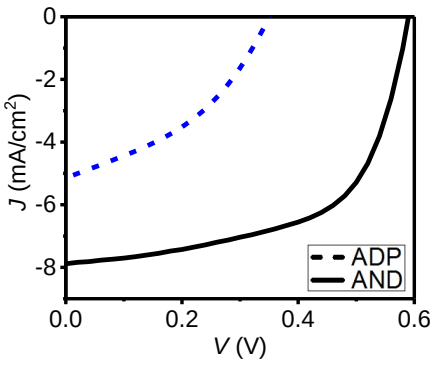

Figure 2.14 *J-V* curves of optimized ADP and AND BL P3HT/PCBM OSCs.

The specific PV characteristics are shown in Fig. 2.15. The huge increments of each J_{sc}, V_{oc} and *FF* by annealing significantly increase the *PCE* from 0.71 to 2.75%. Hence, annealing is an effective way to enhance the performance of ADP BL OSCs. It was reported that the increase of V_{oc} is related to the increase of energy difference between the LUMO of the acceptor and HOMO of the donor.[15,24] In this regard, there is possibility that this energy difference is increased by annealing as shown by the sudden increase of V_{oc} in AND device. Meanwhile, the nanoscale phase separation affected by thermal annealing was said to build percolating network within pure PCBM (more effective charge collection at the electrodes), thus increasing J_{sc} and *FF* in AND device.[24]

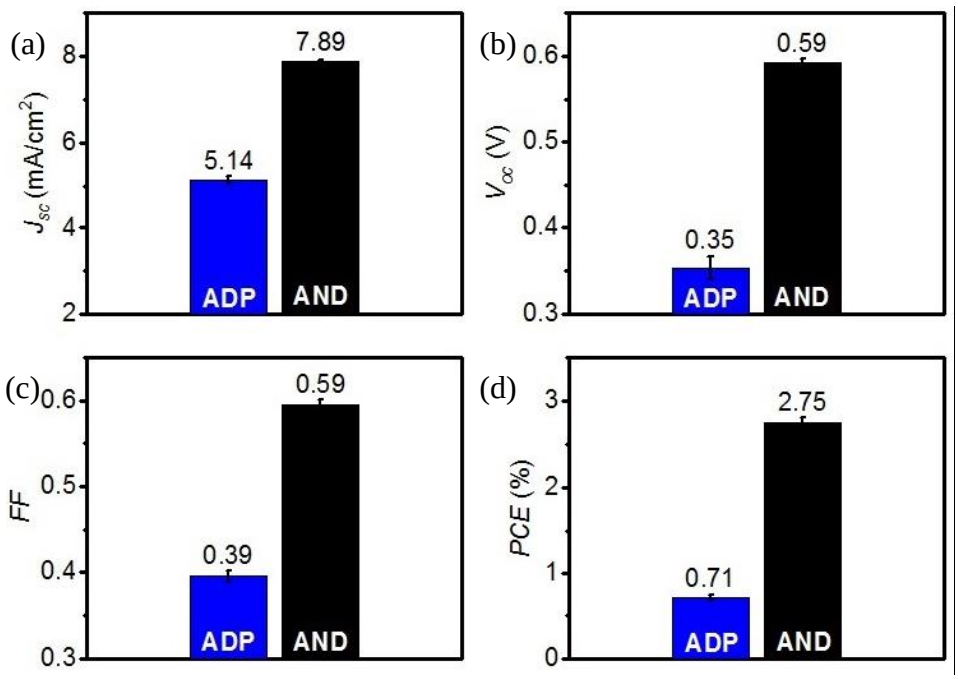

Figure 2.15 Photovoltaic characteristics of as-deposited and annealed bilayer P3HT/PCBM OSCs: (a) J_{sc}, (b) V_{oc}, (c) *FF* and (d) *PCE*.

2.3.7 Morphological, Optical and Structural Analyses of Optimized P3HT Films

The thickness and surface roughness of ADP and AND P3HT films are shown in Figs. 2.16 and 2.17 respectively. After undergoing the post-annealing heat treatment, the thickness of

P3HT film slightly decreases from 50.24 nm to 49.78 nm. Fig. 2.17 shows that the fabricated films feature a spiky surface that indicates the small crystal morphology.[5] Annealing slightly reduced the maximum height of the profile (R_y) from 25.04 to 22.99 nm with the formation of slightly bigger crystals. The slight reduction of film thickness and surface roughness are expected to increase the crystallization and aggregation of AND P3HT film to a certain extent. These properties of individual P3HT film are expected to govern the P3HT/PCBM interface of bilayer devices.

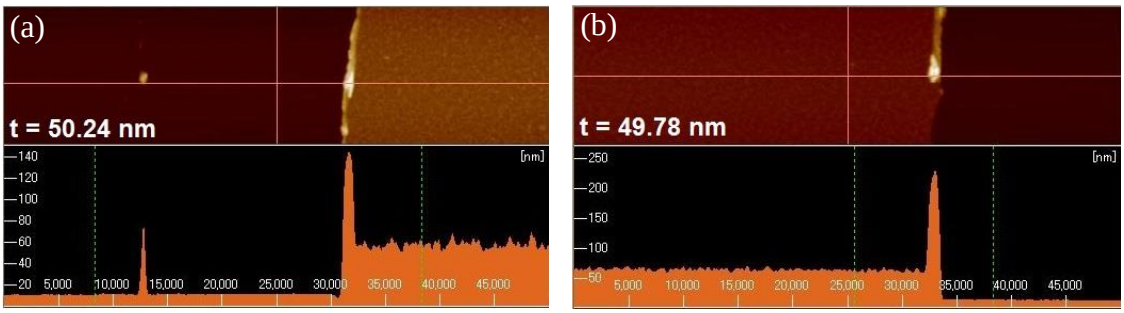

Figure 2.16. Thickness of (a) as-deposited and (b) annealed P3HT films.

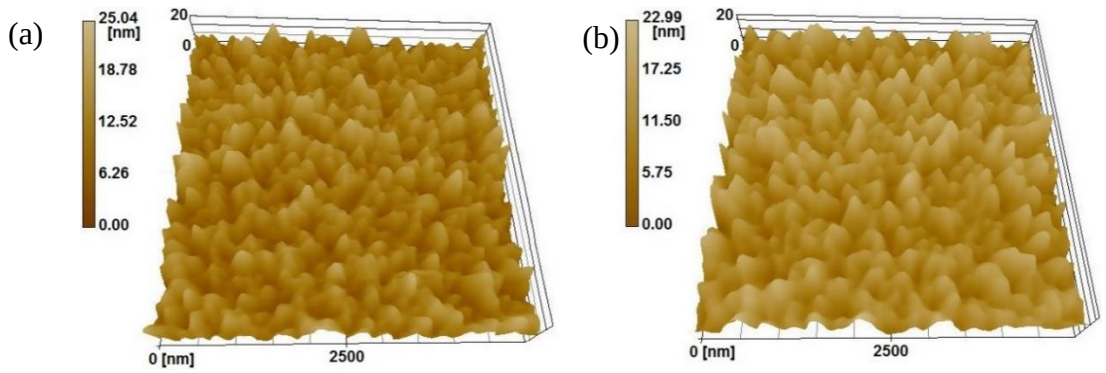

Figure 2.17. AFM images of (a) as-deposited and (b) annealed P3HT films. Each image corresponds to an area of 5 μm × 5 μm.

The optical analysis using UV-visible spectroscopy via absorption coefficient spectra (Fig. 2.7) reveals the onset within the P3HT absorbance spectrum at ca. 600 nm. This reflects the π-π* absorption in which the excitons are generated as the light is absorbed in P3HT film.[25] It

can be observed that both ADP and AND films possess vibronic features in the wavelength range of 500-650 nm. More intense absorption peak at ca. 550 nm and vibronic feature in AND film suggest that this film has more crystallized P3HT domains.[26] This observation matches with the morphological properties in Fig. 2.6 that shows the formation of bigger P3HT domains. Therefore, the enhanced J_{sc} and *FF* in AND device are due to the enhanced absorbance and crystallinity of annealed P3HT film. The higher photon intensity produces larger amount of exciton in the active layer resulting in higher J_{sc} (due to higher exciton dissociation rate).[11] On the other hand, the crystallized P3HT film enhances the transport of photogenerated carriers to the respective electrodes, increasing the *FF*.[5] At the same time, the enhanced V_{oc} is suspected due to the reduced charge recombination as a result of phase separation in annealed device.[24,27]

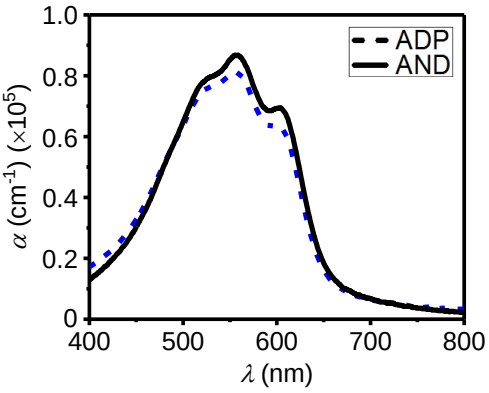

Figure 2.18. Absorption coefficient spectra of ADP and AND P3HT films.

The hole/electron transport in OSCs predominantly takes place in vertical direction to the respectively electrodes.[15,28] A face-on configuration with π-stacking direction normal to the substrate is therefore preferred over the edge-on orientation.[28] pMAIRS was used to investigate the molecular orientation of ADP and AND P3HT films by generating their in-plane (IP) and out-of-plane (OP) infrared (IR) absorbance spectra as shown in Fig. 2.19.

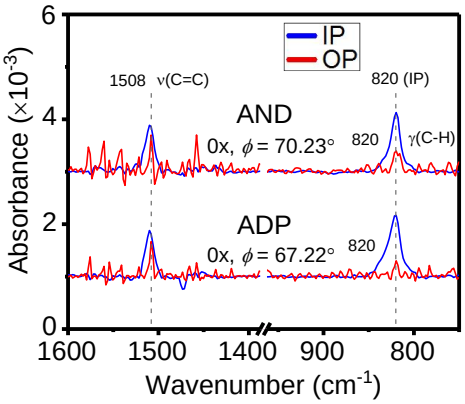

Figure 2.19. The out-of-plane and in-plane pMAIRS spectra of ADP and AND P3HT films.

The thiophene ring vibration [ν(C=C)] mode is assigned at ca. 1510 cm^{-1} wavenumber while the C-H out-of-plane deformation vibration [γ(C-H)] mode on the thiophene ring is designated at ca. 820 cm^{-1} wavenumber.[29] The transition moments of ν(C=C) and γ(C-H) modes serve as the orientation-sensitive marker to estimate the orientation of P3HT molecules.[30] The polymer chain is parallel to ν(C=C) mode while the thiophene ring is perpendicular to γ(C-H) mode.[31] By taking into account the absorbance in OP spectrum (A_{OP}) and the absorbance in IP spectrum (A_{IP}), the orientation angle (ϕ) can be calculated using the following equation.[31]

$$\phi = tan^{-1}\sqrt{\frac{2A_{IP}}{A_{OP}}} \qquad (2.1)$$

The pMAIRS spectra of ADP and AND P3HT films show the presence of dominant ν(C=C) and γ(C-H) modes in the IP spectra, with the measured orientation angles of the γ(C-H) mode from the surface normal, $\phi_{\text{C-H}}$ = 70.23° and 67.22° respectively. These orientation angles indicate that these films have edge-on P3HT molecules.[31] Therefore, the enhanced performance of AND device is not related to the orientation of P3HT molecules where they remain almost unaffected by annealing.

2.4 Summary

The fabrication parameters of BL P3HT/acceptor OSCs have been optimized by varying the substrate cleaning, P3HT solvent, type of electron acceptor, evaporation rate of Al and heat treatment condition. During each optimization step, the other parameters such as the spin-coating speed of P3HT and the cell area were kept constant. It was found that the decent device requires the cleaning process of substrate prior to the deposition of active layer to avoid the impurities. CB should be should as the solvent for P3HT to promote crystalline active layer. Also, $PC_{61}BM$ is chosen acceptor as possessed the optimal crystallinity as exhibited by desirable J_{sc} and *FF* of P3HT/$PC_{61}BM$ OSCs. The evaporation rate of Al will be retained within 7 Å/s to deposit the Al with larger grain size. The post-annealing will be applied for the subsequent device fabrication to ensure optimize the performance of AND device.

The optimized devices were fabricated in ADP and AND conditions by considering the optimized device fabrication parameters for BL P3HT/acceptor OSCs. The characterizations of ADP and AND P3HT films via morphological, optical and structural analyses revealed the reasons behind the enhanced device performance by annealing. The formation of larger well-organized P3HT domains along with its higher absorbance after annealing reflect the crystallization of P3HT film. The crystallization is suspected to occur along with the phase segregation of P3HT/PCBM layer. While the crystallization enhances both J_{sc} and *FF* due to greater exciton formation and enhanced charge transport respectively, the phase separation is expected to increase V_{oc} due to reduced charge recombination (effect of phase segregation). The increases of J_{sc}, *FF* and V_{oc} lead to the significant increase of *PCE* from 0.71% to 2.75%. The effect annealing on P3HT molecular orientation is confirmed by pMAIRS measurement. Annealing was found to slightly affect the orientation of P3HT molecules where the molecular orientation remains being edge-on before and after annealing. The fabrication of optimized BL

P3HT/PCBM OPV devices and P3HT film samples are regarded as the fundamental steps before proceeding with PV performance enhancement by rubbing technique.

2.5 References

1) S. Zheng, X. Deng, and K.Y. Wong, Synth. Met. **162**, 1490 (2012).
2) Z.A. Rahman, K. Sulaiman, A. Shuhaimi, and M. Rusop, Adv. Mater. Res. **501**, 252 (2012).
3) H. Huang and J. Huang, Organic and Hybrid Solar Cells (Springer International Publishing, New York, 2014), pp.1-274.
4) F. Machui, S. Langner, X. Zhu, S. Abbott, and C.J. Brabec, Sol. Energy Mater. Sol. Cells **100**, 138 (2012).
5) V. Vohra, B. Dörling, K. Higashimine, and H. Murata, Appl. Phys. Express **9**, 1 (2016).
6) M. Karakawa, T. Nagai, K. Adachi, Y. Ie, and Y. Aso, J. Mater. Chem. A **2**, 20889 (2014).
7) S. Foster, F. Deledalle, A. Mitani, T. Kimura, K.B. Kim, T. Okachi, T. Kirchartz, J. Oguma, K. Miyake, J.R. Durrant, S. Doi, and J. Nelson, Adv. Energy Mater. **4**, 1 (2014).
8) J.H. Chang, H.F. Wang, W.C. Lin, K.M. Chiang, K.C. Chen, W.C. Huang, Z.Y. Huang, H.F. Meng, R.M. Ho, and H.W. Lin, J. Mater. Chem. A **2**, 13398 (2014).
9) J. Zhao, A. Swinnen, G. Van Assche, J. Manca, D. Vanderzande, and B. Van Mele, J. Phys. Chem. B **113**, 1587 (2009).
10) Y. Liu, J. Zhao, Z. Li, C. Mu, W. Ma, H. Hu, K. Jiang, H. Lin, H. Ade, and H. Yan, Nat. Commun. **5**, 1 (2014).
11) K.A. Mazzio and C.K. Luscombe, Chem. Soc. Rev. **44**, 78 (2014).
12) P.W.M. Blom, V.D. Mihailetchi, L.J.A. Koster, and D.E. Markov, Adv. Mater. **19**, 1551 (2007).
13) H. Ohkita and S. Ito, Polymer (Guildf). **52**, 4397 (2011).
14) A.L. Ayzner, C.J. Tassone, S.H. Tolbert, and B.J. Schwartz, J. Phys. Chem. C **113**, 20050 (2009).
15) V. Vohra, G. Arrighetti, L. Barba, K. Higashimine, W. Porzio, and H. Murata, J. Phys. Chem. Lett. **3**, 1820 (2012).

16) L. Dou, J. You, Z. Hong, Z. Xu, G. Li, R.A. Street, and Y. Yang, Adv. Mater. **25**, 6642 (2013).

17) M.T. Dang, G. Wantz, H. Bejbouji, M. Urien, O.J. Dautel, L. Vignau, and L. Hirsch, Sol. Energy Mater. Sol. Cells **95**, 3408 (2011).

18) K. Bordo and H.G. Rubahn, Mater. Sci. **18**, 313 (2012).

19) G. Kalonga, G.K. Chinyama, M.O. Munyati, and M. Maaza, J. Chem. Eng. Mater. Sci. **4**, 93 (2013).

20) J.C. Bernède, J. Chil. Chem. Soc. **53**, 1549 (2008).

21) T.S. Glen, N.W. Scarratt, H. Yi, A. Iraqi, T. Wang, J. Kingsley, A.R. Buckley, D.G. Lidzey, and A.M. Donald, J. Polym. Sci. Part B Polym. Phys. **140**, 25 (2015).

22) B.W. Guralnick, J.E. Seppala, and M.E. MacKay, J. Polym. Sci. Part B Polym. Phys. **49**, 772 (2011).

23) C. Deibel and V. Dyakonov, Reports Prog. Phys. **73**, 96401 (2010).

24) M. Al-Ibrahim, O. Ambacher, S. Sensfuss, and G. Gobsch, Appl. Phys. Lett. **86**, 1 (2005).

25) J. Müllerová, M. Kaiser, V. Nádaždy, P. Šiffalovič, and E. Majková, Sol. Energy **134**, 294 (2016).

26) Y. Jang, J.W. Seo, J. Seok, J.Y. Lee, and K. Kim, Polymers **7**, 1497 (2015).

27) B.G. Kim, E.J. Jeong, H.J. Park, D. Bilby, L.J. Guo, and J. Kim, ACS Appl. Mater. Interfaces **3**, 674 (2011).

28) W. Huang, E. Gann, L. Thomsen, C. Dong, Y.B. Cheng, and C.R. McNeill, Adv. Energy Mater. **5**, 1401259 (2015).

29) N. Shioya, T. Shimoaka, K. Eda, and T. Hasegawa, Phys. Chem. Chem. Phys. **17**, 13472 (2015).

30) N. Shioya, T. Shimoaka, and T. Hasegawa, Chem. Lett. **43**, 1198 (2014).

31) N. Shioya, T. Shimoaka, K. Eda, and T. Hasegawa, Macromolecules **50**, 5090 (2017).

Chapter 3

ENHANCEMENT OF PHOTOVOLTAIC PERFORMANCE OF BILAYER OSCs BY RUBBING TECHNIQUE

3.1 Introduction

There are variety of methods that can be applied to enhance the performance of BL OPV devices including the use of high performance donor and acceptor materials[1,2], the optimization of device fabrication parameters[3,4] and the adjustment of the properties of the active layer[5,6] of the device. BL architecture provides the possibility to enhance the properties of the donor layer of the device.[7] With the regular configuration of BL device geometry, the treatment of donor layer would induce the changes at the donor/acceptor interface. These changes may involve the morphological, compositional and structural properties of the active layers.

The donor layers have been individually treated by various methods such as the solvent variation[8], additive introduction[9] and application of rubbing technique[6]. Rubbing is the feasible method to adjust the properties of the P3HT donor layers. By using a piece of soft rubbing material, this technique can be easily performed by hand without relying on the costly chemicals and equipment. Depending upon the features of P3HT (e.g. molecular weight and regioregularity), the use of rubbing was said to be capable of altering the properties of P3HT film including its surface roughness, absorbance, crystallinity and molecular orientation. In this regard, rubbing is promising to enhance the PV performance of the BL OPV cells. The understanding and modification of rubbing technique is anticipated to give the positive impact on the device performance.

3.1.1 Rubbing Technique

Rubbing is the application of pressure against the surface of a thin film material at a particular direction. Due to its ability to alter the morphology and induce molecular orientation of organic semiconductor film, rubbing technique has been applied on organic optoelectronic devices including organic light emitting diode[10], organic field effect transistor[11] and OPV devices.[6,12] This technique is expected to be widely used for the fabrication of OPV cells by its ability to improve the in-plane carrier transport of oriented conjugated polymer film.[6,13] It was reported that rubbing low regioregular P3HT (RR-P3HT) films causes the molecular orientation of their backbone chains parallel to the rubbing direction and their structure of crystalline domains change from edge-on to face-on orientation.[6,14] The increase of face-on crystallites corresponds to the increase of π-π stacking of thiophene ring along the out-of-plane direction.[13] The face-on crystallite configuration was reported to induce the better charge transport in the vertical direction.[6,15] The vertical direction of charge transport is more favourable for OPV as the dissociated charges at the interface need to percolate to their respective electrodes.[1,15] Owing to its ability to align the molecular orientation of conjugated polymer layer individually, the applicability of this technique has been mostly carried out on conventional bilayer device architecture.[6,16]

3.2 Experimental Procedure

3.2.1 Development of Rubbing Technique

The initial stage of the implementation of rubbing technique involved the application of manual rubbing by adjusting the feasible parameters such as rubbing step and direction. The rubbing process was manually performed in such a way that the polymeric thin films facing upwards were rubbed by either nylon cloth or velvet cloth.[6,13,17] However, the details of rubbing

technique remain ambiguous as there is lack of quantitative control in rubbing parameters such as rubbing pressure, speed and distance. The conventional approach of rubbing was improved by introducing the auto-controllable pressure loads system over the manual approach. The comparative study of both manual and automatic rubbing processes was provided to scrutinize the effect of applied rubbing pressures on the PV performance of P3HT/PCBM OPV devices.

Throughout the development of rubbing technique, nylon cloth has been used as the main rubbing medium. Initially, the folded nylon cloth (Fig. 3.1a) was used as a rubbing medium to manually rub the sample. The nylon cloth used is a kind of composite wiping cloth (Savina MX, KB Seiren, Ltd.) composed of polyester and nylon. As a result of the split open knit polyester/nylon composite yarn, there is a high filament density (82,550 filaments/cm^2) on the cloth surface. By using this rubbing approach, the applied rubbing force could possibly be erratic as the area of folded nylon cloth is not constant. Instead of simply folding the nylon, the use of a fixture to support the nylon cloth during the rubbing process could be the good approach. With this idea, Rubbing Tool 2 (Fig. 3.1b) was developed by forming the fixture made from a 3D printer. Subsequently, the rubbing tool was further developed with the use of a miniature suspension system (Fig. 3.1c) to hold the sample flexibly. The organic layers were arranged to face downwards and rubbed on the affixed nylon cloth underneath. For the purpose of measuring the rubbing pressure, the inverted setup of rubbing was employed where the sample is hold upside down (the organic layer is facing the nylon cloth). The sample has the fixed area (2.5 cm × 2.5 cm) which is required for the estimation of rubbing pressure. To hold the sample more consistently, the auto-rubbing technique (Fig. 3.1d) was developed by employing a modified desktop robot in order to hold and move the sample consistently in three-dimensional directions via its controller. In this manner, the sample is the moving component while the nylon cloth remains static during the rubbing process. Using this auto-rubbing, the applied rubbing pressure can be estimated by calibrating the applied load on the electronic weigher beforehand. The use of desktop robot is expected to realize the better control of

rubbing parameters (e.g. rubbing pressure, speed and distance) as this device does not vibrate nor change the pressure during the movement of the sample. However, the problem occurred during the rubbing where the sample intermittently stuck on the nylon cloth during the rubbing process. To overcome this issue, further work to enhance the rubbing tool is necessary. In the present work, the folded nylon cloth was reused with a clip (Fig. 3.1e). The clip firmly holds the folded nylon cloth during the rubbing process. The nylon cloth is folded and clipped at ca. 0.8 cm height (from the edge of the clip to the point of contact between the samples and the nylon cloth) to ensure the consistency of rubbing pressure.

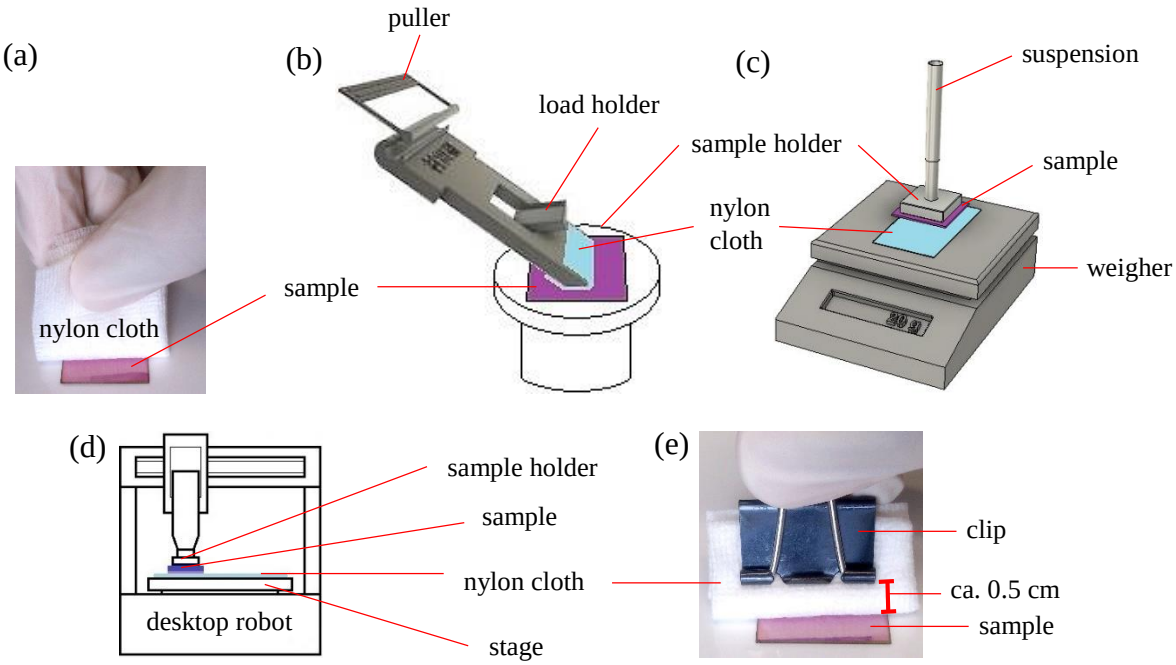

Figure. 3.1. The development stages of rubbing technique: (a) folded nylon cloth, (b) Rubbing Tool 2, (c) Rubbing Tool 3 , (d) automatic rubbing device and (e) clipped nylon cloth.

3.2.2 Fabrication Process of Rubbed P3HT Films and P3HT/PCBM OSCs

To prepare the bilayer P3HT/PCBM OPV devices, ITO-coated glass substrates were ultrasonically cleaned in acetone, detergent, pure water and IPA. After undergoing the UV-ozone treatment for 30 min, they were moved into the nitrogen-filled glove box. The hole

transport interlayer (30 nm) was deposited by spin coating the PEDOT:PSS solution on the cleaned substrates at 4000 rpm for 30 s. P3HT was dissolved in CB at 30 mg/mL. This solutions were stirred at 50 °C, 200 rpm for ca. 3 hrs. P3HT films were prepared by spin coating the P3HT solutions at 2500 rpm, for 30 s. The P3HT films were uniaxially rubbed with nylon cloth for 10 times using different approaches of rubbing (Fig 3.1). The rubbing at different rubbing pressures was performed using the manual-rubbing (Fig. 3.1c) and auto-rubbing (Fig. 3.1d) . The rubbing pressure was varied to 0.63 and 2.51 kN/m^2, corresponding to the loads of 40g and 160g respectively. Note that the control of rubbing pressure by manual-rubbing may not be accurate because it was roughly estimated by rubbing the P3HT films on a weigher. The PCBM powder was dissolved in DCM solvent to obtain 10 mg/mL PCBM solution. This acceptor solution was spin-coated on P3HT layer at 4000 rpm for 10 s to prepare ca. 24 nm-thick PCBM layer. To prepare the samples of P3HT films, quartz substrates were used instead of ITO-coated glass substrates. The preparation of active layers was done in a glove box filled nitrogen containing oxygen at a concentration of less than 1%. Using the vacuum evaporator, Al electrode (100 nm) was deposited at evaporation rate of ca. 3 Å/s. The encapsulation process was carried in a glove box with an oxygen concentration of less than 1 ppm to protect the active layers and electrodes from oxidation. The BL P3HT/PCBM devices having four cells each with 4 mm^2 area were fabricated.

3.3 Results and Discussion

3.3.1 Effect of rubbing by Folded Nylon Cloth and Rubbing Tool 2 on The Photovoltaic Performance of Bilayer P3HT/PCBM OSCs

Rubbing was initially performed using a folded nylon cloth as a rubbing medium. With the aim to support the nylon cloth during the rubbing process, Rubbing Tool 2 was developed and used for rubbing. By using these two approaches, two batches consisting of unrubbed and 10 times-

rubbed devices were fabricated separately. In view to compare the device performances of these two batches, the PV performances of these devices were measured using the solar cell simulator.

As shown in Fig. 3.2, the *J-V* curves indicate the effect of rubbing using folded nylon cloth (FNC) and Rubbing Tool 2 (RT2) on the PV performance of P3HT/PCBM bilayer OPV devices. The details of the PV characteristics are shown in Tables 3.1-3.2 and Fig. 3.3. In as-deposited (ADP) condition, except for the V_{oc}, the PV performances of two unrubbed devices are not comparable. This indicates the poor reproducibility of device performance that could be attributed to the inconsistent experimental handling and the surrounding factors (e.g. room temperature and humidity). Rubbing by folded nylon cloth significantly increases the J_{sc} along with the increases of V_{oc} and *FF*. Rubbing by Rubbing Tool 2, however, slightly reduces the J_{sc} despite of increasing the V_{oc} and *FF*. These phenomena bring about more significant increase of *PCE* in FNC-rubbed device (from 0.76% to 1.54%) as compared to that of RT2-rubbed device (from 1.01% to 1.11%). Despite of the similar 10 times rubbing number, the different ways of rubbing yield distinct increments of PV characterisctis. This could be due to the different pressure exerted on the P3HT films by folded nylon cloth and Rubbing Tool during the rubbing process. The high pressure exerted on the P3HT film could have altered its morphology (i.e. increase surface roughness), thereby increasing the P3HT/PCBM interface after PCBM deposition on the P3HT layer. The increased P3HT/PCBM interfacial area increases the charge generation rate which is related to the increased PV characteristics. In this regards, the pressure exerted by folded nylon cloth is presumed to be higher than that of Rubbing Tool 2.[18,19] In conjunction with that, the proper control of the rubbing pressure could be beneficial in achieving the decent device performance.

In case of annealed devices, rubbing by folded nylon cloth reduces the J_{sc} while retaining the increases of V_{oc} and *FF*. The increase of *FF* is relatively higher than that of V_{oc}, thus *FF* dominantly affects the increase of *PCE* of FNC-rubbed device from 2.24% to 2.73%. On the

other hand, rubbing by Rubbing Tool 2 results in less striking enhancement of the device performance due to relatively small increases of its J_{sc}, V_{oc} and *FF*. Consequently, the *PCE* of RT2-rubbed device increases from 2.10% to 2.25%. The crystallization and phase segregation of active layer after annealing could have affected the effectiveness of rubbing in improving the PV performance of AND devices.[19,20]

The approach of rubbing technique is important to achieve the favorable performance of rubbed bilayer OPV device. By comparing the PV performance of FNC-rubbed and RT2-rubbed devices, the folded nylon cloth for rubbing should simply be used for the rubbing process. Additionally, the distinctive performances of FNC-rubbed and RT2-rubbed devices leads to the attempt of controlling the rubbing pressure which could be achieved by modifying the rubbing tool.

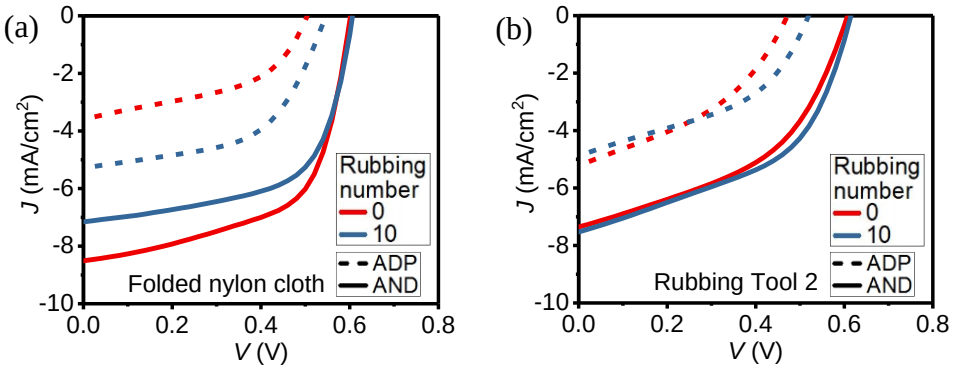

Figure. 3.2 *J-V* curves of unrubbed and 10 times-rubbed P3HT/PCBM OPV devices with the use of (a) folded nylon cloth and (b) Rubbing Tool 2 for rubbing.

Table 3.1 PV characteristics of unrubbed and 10 times-rubbed P3HT/PCBM OPV devices with the use of folded nylon cloth as rubbing medium.

Rubbing number	J_{sc} (mA/cm^2)		V_{oc} (V)		*FF*		*PCE* (%)	
	ADP	AND	ADP	AND	ADP	AND	ADP	AND
0	3.28	6.72	0.49	0.59	0.45	0.56	0.76	2.24
10	5.16	6.51	0.55	0.61	0.55	0.70	1.54	2.73

Table 3.2 PV characteristics of unrubbed and 10 times-rubbed P3HT/PCBM OPV devices with the use of Rubbing Tool 2 for rubbing.

Rubbing number	J_{sc} (mA/cm^2)		V_{oc} (V)		*FF*		*PCE* (%)	
	ADP	AND	ADP	AND	ADP	AND	ADP	AND
0	5.22	7.32	0.49	0.61	0.39	0.47	1.01	2.10
10	4.87	7.52	0.53	0.62	0.43	0.48	1.11	2.25

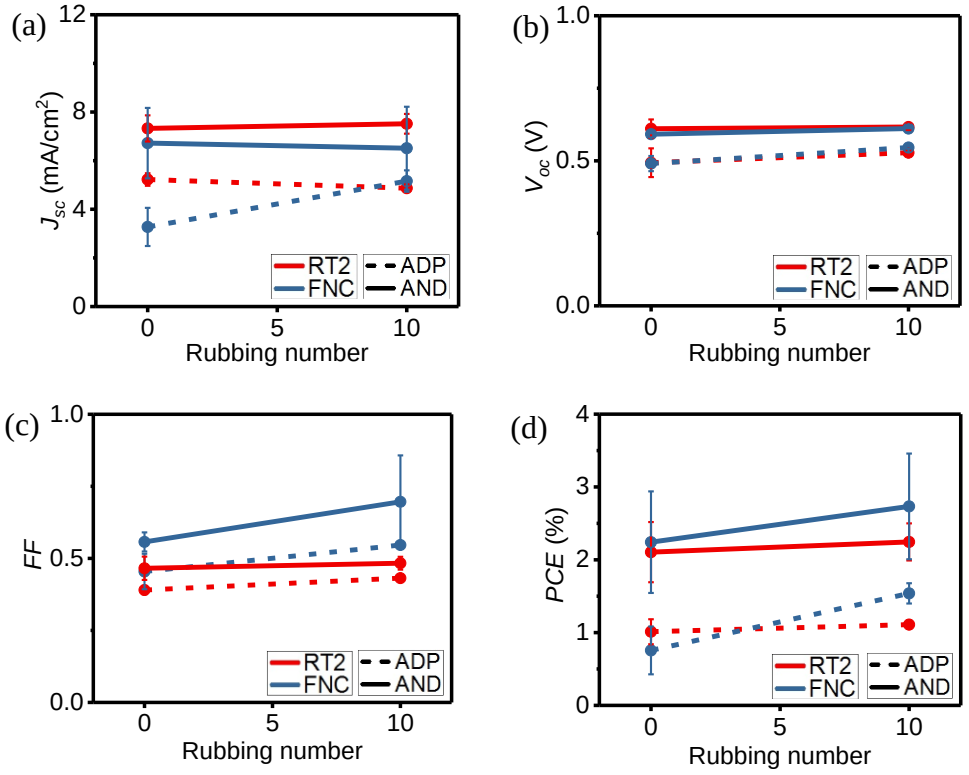

Figure 3.3 Photovoltaic performance of unrubbed and 10 times-rubbed P3HT/$PC_{61}BM$ OPV devices: (a) J_{sc}, (b) V_{oc}, (c) *FF* and (d) *PCE* with the use of folded nylon cloth and Rubbing Tool 2 for rubbing.

3.3.2 Effect of Different Rubbing Pressures by Manual and Automatic Rubbing on The Photovoltaic Performance of Bilayer P3HT/PCBM OSCs

In this section, manual rubbing (MR) is referred to the rubbing process using Rubbing Tool 3 (RT3) (Fig. 3.1c) while automatic rubbing (AR) referred to the rubbing process using the modified desktop robot (Fig. 3.1d). The batches of manual-rubbed and auto-rubbed devices

were fabricated separately where the P3HT films were rubbed for 10 times uniaxially. In case of the ADP devices, the *J-V* curves (Fig. 3.4) and the comparison of device performance (Tables 3.3-3.4 and Fig. 3.5) show that the PV performances of unrubbed devices are not comparable, possibly due to their inconsistent experimental procedures. The waiting time prior to the aluminum evaporation is suspected to control the drying process of the active layer. The device with longer drying process would have more crystalline active layer which absorbs more photon[21] for the favorable J_{sc}. The automatic rubbing results in higher J_{sc} as compared to that of manual rubbing. This is possibly due to the rougher surface of auto-rubbed P3HT film that induces larger surface area at P3HT/PCBM interface for better light absorption.[9] On the other hand, the manual rubbing results in the steady increase of V_{oc} and better *FF* in the devices, as compared to that of auto-rubbed devices. This could be attributed to the favorable intermixing at the interface of P3HT and PCBM layer of the manual-rubbed devices that reduces the charge recombination and increases the charge collection at the electrodes.[22,23]

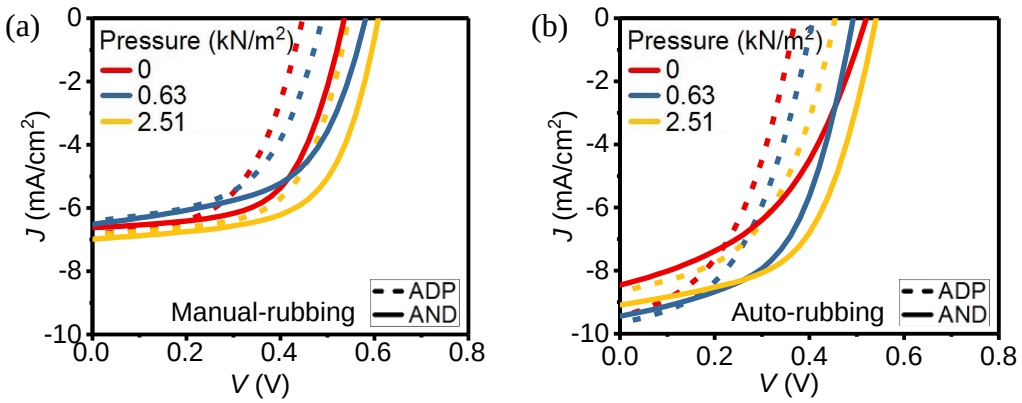

Figure. 3.4 *J-V* curves of (a) manual-rubbed and (b) auto-rubbed P3HT/PCBM OPV devices with respect to different rubbing pressures.

As for the AND devices, there is almost no change of J_{sc} of both manual-rubbed and auto-rubbed devices. On contrary, there are notable increases of V_{oc} in these devices. The increase of *FF* more significant in auto-rubbed device. The phase segregation and the increased

crystallinity by annealing are suspected to influence the J_{sc}, V_{oc} and *FF* in manual-rubbed and auto-rubbed AND devices.[19,20] The phase segregation might not be able to increase the P3HT/PCBM interface due to an unknown reason, thus retaining the increase of J_{sc}. Meanwhile, the aforementioned effect of rubbing could have reduced the recombination loss and enhanced the charge transport in the active layers.[23] The phenomena contribute to the increases of V_{oc} and *FF*.

Table 3.3 PV characteristics of manual-rubbed P3HT/PCBM OPV devices corresponding to different rubbing pressures.

Rubbing pressures (kN/m^2)	J_{sc} (mA/cm^2)		V_{oc} (V)		*FF*		*PCE* (%)	
	ADP	AND	ADP	AND	ADP	AND	ADP	AND
0	6.48	6.57	0.46	0.54	0.53	0.59	1.59	2.09
0.63	6.13	6.39	0.50	0.59	0.54	0.56	1.66	2.11
2.51	6.52	6.55	0.54	0.61	0.61	0.62	2.15	2.50

Table 3.4 PV characteristics of auto-rubbed P3HT/PCBM OPV devices corresponding to different rubbing pressures.

Rubbing pressures (kN/m^2)	J_{sc} (mA/cm^2)		V_{oc} (V)		*FF*		*PCE* (%)	
	ADP	AND	ADP	AND	ADP	AND	ADP	AND
0	9.01	8.29	0.38	0.50	0.44	0.45	1.54	1.95
0.63	9.43	9.38	0.42	0.50	0.46	0.52	1.79	2.43
2.51	9.31	9.48	0.42	0.51	0.46	0.51	1.87	2.62

The comparison of the PV performances of manual-rubbed and auto-rubbed devices imply that the control of rubbing pressure is practical to be used to enhance the device performance. The increase of rubbing pressure from 0.63 to 2.51 kN/m^2 leads to the increases of almost all of PV characteristics of ADP and AND devices. The control of rubbing pressure is seen to be more feasible by employing the auto-rubbing device. However, the enhancement of the photovoltaic performance of auto-rubbed devices indicates that the automatic rubbing

approach is not fully consistent yet and requires further improvement. One of the challenges of the automatic rubbing is the control of the tilting angle between the sample and the stage of nylon cloth. The improper control of this angle would result in the non-uniform application of rubbing on the P3HT films as shown in Fig. 3.6. During the fabrication of rubbed device, such kind of non-uniform P3HT films were not observed. This approach of rubbing could not be able to reproduce the samples with the consistent rubbing pressures. Consequently, the simple approach of rubbing by the folded using nylon cloth is re-considered as described in the subsequent section.

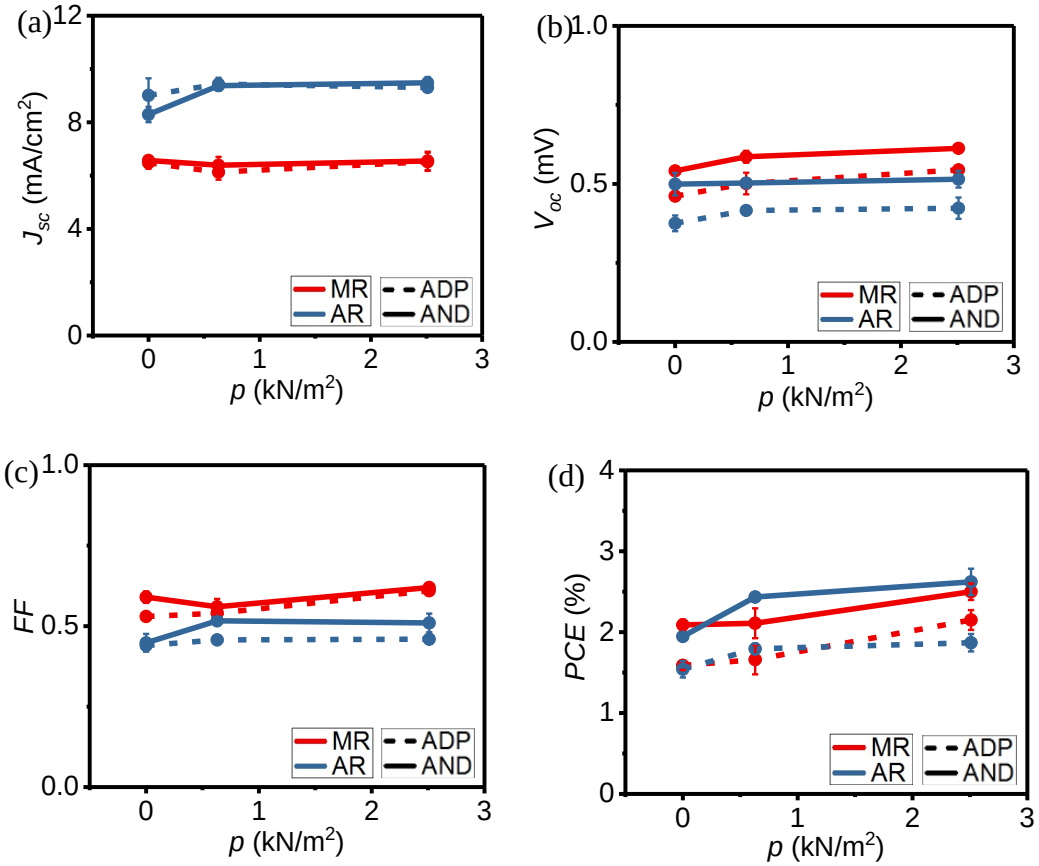

Figure 3.5 Photovoltaic performance of manual-rubbed and auto-rubbed P3HT/$PC_{61}BM$ OPV devices: (a) J_{sc}, (b) V_{oc}, (c) *FF* and (d) *PCE* corresponding to different rubbing pressures (MR: manual-rubbing; AR: auto rubbing).

(a)  (b) 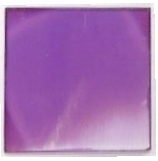 (c) 

Figure 3.6 The samples rubbed by auto-rubbing: (a) unrubbed, (b) 0.63 kN/m^2-rubbed and (c) 2.51 kN/m^2-rubbed samples. Sample size: 2.5 cm × 2.5 cm.

3.3.3 Effect of Rubbing by Clipped Nylon Cloth on The Photovoltaic Performance of P3HT/PCBM Bilayer OSCs.

The rubbing process using the folded nylon cloth is re-considered as a result of the unfavourable control of rubbing pressure using the Rubbing Tool 3 and automatic rubbing device to reproduce the rubbing pressure. A clip is used to hold the folded nylon cloth. The clipped nylon cloth (Fig. 4.1e) with the distance from the tip of the clip and the tip of the folded nylon cloth of ca. 0.5 cm ensures that the consistency of the applied rubbing pressure. The *J-V* curves (Fig. 4.7), Table 4.5 and Fig. 4.8 show the significant increases of J_{sc} and V_{oc} in the rubbed ADP device with the slight increase of *FF*. The clipped nylon cloth (CNC)-rubbed device has *PCE* of 1.26% which is a notable increase over 0.71% *PCE* of the unrubbed device. The application rubbing could give dominant treatment on the morphology of the semi-crystalline P3HT layer which affects the diffusion of PCBM during its spin coating. The compositional studies would uncover the huge increment of each PV characteristic of CNC-rubbed ADP device.

Annealing substantially enhances PV performance the unrubbed device where the *PCE* increases from 0.71% to 2.75%. Despite of the small increases of V_{oc} and *FF* of rubbed AND, the slight reduction of J_{sc} restricts the enhancement of the device performance by rubbing where the PCE increases from 2.75 to 2.90%. The segregation of the annealed active layer might have slightly reduce the P3HT/PCBM interface of rubbed device, resulting in the small decrease of J_{sc}.[19] The crystallization of the annealed active layer suggests that the reduced

charge recombination and improved charge transport contribute to the enhanced V_{oc} and *FF* of the AND devices.[22]

The PV performance of the unrubbed and CNC-rubbed devices in ADP and AND conditions shows that rubbing is relatively effective on the ADP devices. Annealing is capable to significantly enhance the PV characteristics of the annealed device. At the same time, it is observed to hinder the effect of rubbing on the enhancement of the device performance.

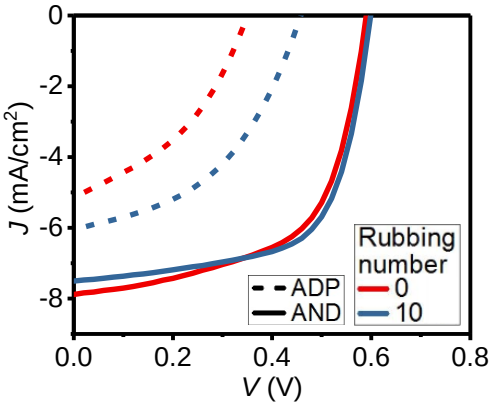

Figure. 3.7 *J-V* curves of unrubbed and 10 times-rubbed P3HT/PCBM OPV devices with the use of clipped nylon cloth as rubbing medium.

Table 3.5 PV characteristics of unrubbed and 10 times-rubbed P3HT/PCBM OPV devices with the use of clipped nylon cloth as rubbing medium.

Rubbing number	J_{sc} (mA/cm^2)		V_{oc} (V)		*FF*		*PCE* (%)	
	ADP	AND	ADP	AND	ADP	AND	ADP	AND
0	5.14	7.89	0.35	0.59	0.39	0.59	0.71	2.75
10	6.04	7.51	0.45	0.60	0.45	0.64	1.26	2.90

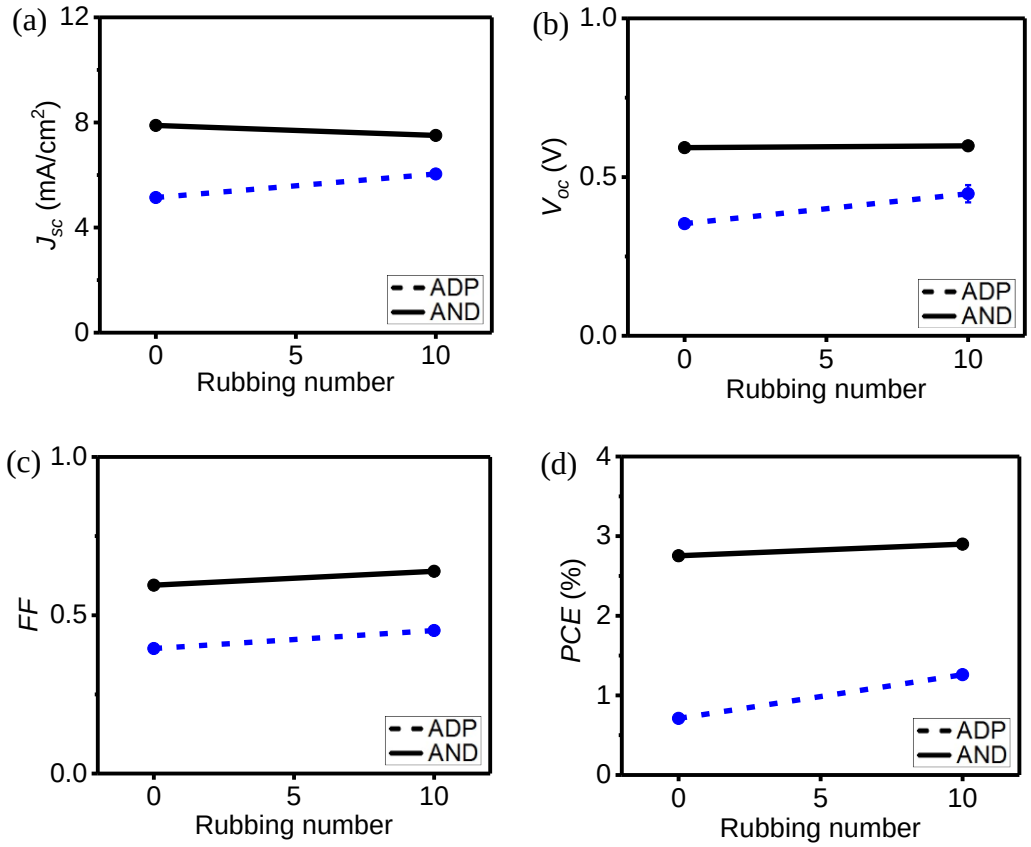

Figure 3.8 Photovoltaic performance of unrubbed and 10 times-rubbed P3HT/$PC_{61}BM$ OPV devices: (a) J_{sc}, (b) V_{oc}, (c) *FF* and (d) *PCE* with the use of clipped nylon cloth as rubbing medium.

3.4 Summary

The attempt to obtain the decent performance of the rubbed bilayer devices was carried out using P3HT and PCBM as the donor and acceptor materials, respectively. The use of folded nylon cloth and Rubbing Tool 2 to fabricate the rubbed bilayer OPV devices leads to the attempt to further modify the approach of rubbing. The inability to reproduce the consistent rubbing pressure via automatic rubbing device causes the folded nylon cloth to be reused as the rubbing medium. The decent PV performance with *PCE* of 2.90% is realized by employing the clipped nylon cloth for rubbing and post-annealing heat treatment. With its applicability and positive impact on P3HT layer, rubbing is believed to be a feasible technique to enhance the bilayer OPV cells. Since rubbing involves the treatment of the P3HT/PCBM interface, the

thorough understanding about the morphology and composition of the whole active layer is necessary to explain the mechanisms behind the individual effect of rubbing and annealing on the PV performance of bilayer OPV devices. The related characterizations and the reproducibility of the device performance will be covered in the subsequent chapter.

3.5 References

1) Y. Yang, W. Chen, L. Dou, W.-H. Chang, H.-S. Duan, B. Bob, G. Li, and Y. Yang, Nat. Photonics **9**, 1 (2015).
2) M. Karakawa, T. Nagai, K. Adachi, Y. Ie, and Y. Aso, J. Mater. Chem. A **2**, 20889 (2014).
3) W. Zhao, S. Li, H. Yao, S. Zhang, Y. Zhang, B. Yang, and J. Hou, J. Am. Chem. Soc. **139**, 7148 (2017).
4) G. Kalonga, G.K. Chinyama, M.O. Munyati, and M. Maaza, J. Chem. Eng. Mater. Sci. **4**, 93 (2013).
5) V. Vohra, O. Notoya, T. Huang, M. Yamaguchi, and H. Murata, Polym. (United Kingdom) 55, 2213 (2014).
6) V. Vohra, G. Arrighetti, L. Barba, K. Higashimine, W. Porzio, and H. Murata, J. Phys. Chem. Lett. **3**, 1820 (2012).
7) A.L. Aysner, C.J. Tassone, S.H. Tolbert, and B.J. Schwartz, J. Phys. Chem. C **113**, 20050 (2009).
8) V. Vohra, B. Dörling, K. Higashimine, and H. Murata, Appl. Phys. Express **9**, 1 (2016).
9) Y. Jang, J.W. Seo, J. Seok, J.Y. Lee, and K. Kim, Polymers **7**, 1497 (2015).
10) T. Matsushima, and H. Murata, J. Appl. Phy. **112**, 24503 (2012).
11) H. Heil, T. Finnberg, N.V. Malm, R. Schmechel, and H.V. Seggern, J. Appl. Phys. **93**, 1636 (2003).
12) L. Huang, H. Liu, T. Chou, J. Hsieh, W. Chiu, L. Wang, and C.-Y. Chao, J. Phys. Sci. Appl. **4**, 475 (2014).
13) D. Kajiya, S. Ozawa, T. Koganezawa, and K.I. Saitow, J. Phys. Chem. C **119**, 7987 (2015).
14) L. Hartmann, K. Tremel, S. Uttiya, E. Crossland, S. Ludwigs, N. Kayunkid, C. Vergnat, and M. Brinkmann, Adv. Funct. Mater. **21**, 4047 (2011).

15) V. Skrypnychuk, N. Boulanger, V. Yu, M. Hilke, S.C.B. Mannsfeld, M.F. Toney, and Barbero, Adv. Funct. Mater. **25**, 664 (2015).

16) Y.H. Huh, I.G. Bae, H.G. Jeon, and B. Park, Opt. Express **24**, 1321 (2016).

17) R. Zhu, A. Kumar, and Y. Yang, Adv. Mater. **23**, 4193 (2011).

18) H. Ohkita and S. Ito, Polymer **52**, 4397 (2011).

19) K.A. Mazzio and C.K. Luscombe, Chem. Soc. Rev. **44**, 78 (2014).

20) V.S. Gevaerts, L.J.A. Koster, M.M. Wienk, and R.A.J. Janssen, ACS Appl. Mater. Interfaces **3**, 3252 (2011).

21) X. Lin, J. Seok, S. Yoon, T. Kim, and K. Kim, Synth. Met. **196**, 145 (2014).

22) S.B. Hacène and T. Benouaz, Phys. Status Solidi Appl. Mater. Sci. **211**, 862 (2014).

23) B.G. Kim, E.J. Jeong, H.J. Park, D. Bilby, L.J. Guo, and J. Kim, ACS Appl. Mater. Interfaces **3**, 674 (2011).

Chapter 4

REPRODUCIBLE DEVICE PERFORMANCE AND EFFECT OF RUBBING ON THE PERFORMANCE OF OSCs

4.1 Introduction

The fabrication of OPV device commonly involves the solution processes such as screen printing, inkjet printing, doctor blading and spin coating. Spin coating has been the feasible deposition method for the small-scale device fabrication where it is often used for research purpose. Though the device fabrication scale is small, it is fundamentally important for the operator to be well-versed with the experimental handling and device fabrication procedures to realize the bilayer OPV devices with reproducible PV performance. The performance of the bilayer devices is aimed to be further improved by employing the rubbing technique. The reproducibility of their performance allows the regular unrubbed device to be benchmarked with the other batch of the devices.

4.1.1 Factors Causing the Poor Device Performance Reproducibility

Organic material such as the conjugated polymer (i.e. P3HT) is known to be very sensitive and easily degrades in the presence of water and oxygen. To form the P3HT film via solution process (i.e. spin coating), P3HT is usually dissolved in a specific solvent based on its solubility in the solvent and the boiling point of the solvent. Considering the experimental procedures that involve the use of various organic solvents and materials, very thorough handling should be taken into account during the experiment. Besides, the consistency of the experimental handling is another factor that needs to be considered to fabricate the devices with reproducible

performance. This is because the evaporation of the spin coated conjugated solution may affect the diffusion of upper PCBM layer.

4.1.2 Vertical Concentration Gradient and Molecular Orientation on BL P3HT/PCBM OSCs

It has been well known that it is difficult to control the nanomorphology of BHJ active layer in large-area film deposition. Thus, BL approach is much more promising for commercial production of OSCs. Some studies argued that similar concentration gradients and nanomorphologies are produced both BHJ and BL active layers upon subjected to heat treatment.[1–3] Graded BLs prepared through sequential solvent deposition exhibit a great potential for highly efficient and stable OSCs fabrication provided that the sufficient donor-acceptor vertical concentration profiles are formed. Rubbing P3HT film before PCBM deposition was reported to improve the performances of AND BL OSCs.[4] In addition, such application of rubbing has been demonstrated to change the molecular orientation of P3HT molecules from edge-on to face-on configuration.[4,5] The change of molecular orientation from edge-on to face-on crystallites brings about intermolecular charge transport, improving the charge collection efficiency in the vertical direction normal to the electrodes of the BL OSCs.[4,6] To complement the past investigation on AND BL OSCs, this chapter will ultimately confirm whether the enhanced thin film properties are due to rubbing, annealing or a synergy of both processes.

4.2 Experimental Procedure

4.2.1 Fabrication Process of Reproducible Bilayer P3HT/PCBM OSCs

The glass substrates coated with indium tin oxide (ITO) were ultrasonically cleaned in acetone, Semico clean, pure water and isopropyl alcohol (IPA). Then, they were subjected to the UV-

ozone treatment for 30 min. The hole transport interlayer was deposited by spin coating the poly(3,4-ethylenedioxythiophene)-poly(styrenesulfonate) (PEDOT:PSS) solution (Heraeus, Clevious P VP AI 4083) on the cleaned substrates at 4000 rpm for 30 s. P3HT powder (BASF Sepiolid P200, >98% RR) was dissolved in CB to prepare 30 mg/mL P3HT solution. This solution was stirred at 200 rpm, 50 °C for ca. 3 hr. The spin coating of P3HT solution was performed at 2500 rpm for 30 s. The PCBM powder (Luminescence Technology) was dissolved in DCM solvent to obtain 10 mg/mL PCBM solution. This acceptor solution was spin-coated on P3HT layer at 4000 rpm for 10 s. Using the vacuum evaporator, Al electrode was deposited at evaporation rate of ca. 7 Å/s. The encapsulation process was carried out after the Al evaporation to protect the devices from the moisture. The inert atmosphere (nitrogen-filled with <1% oxygen concentration) was retained from the preparation of active layers until the device encapsulation.

The photovoltaic performance of the ADP P3HT/PCBM devices was measured using Keithley 2400 Sourcemeter paired with the solar simulator under 1 sun (AM1.5G, 100 mW cm^{-2}) irradiation. Then, the devices were annealed at 140 °C for 10 min. After that, the measurement of photovoltaic performance was repeated to get the photovoltaic characteristics of AND devices.

4.2.2 Fabrication Process and Characterization of Rubbed Bilayer P3HT/PCBM OSCs and P3HT Films

Basically, the procedures from the substrates cleaning up to P3HT spin coating exactly follow the previous procedures to fabricate the unrubbed devices. To prepare the rubbed devices, the P3HT films were uniaxially rubbed as-cast without further drying. They were rubbed for 5, 10, 15 and 20 times by hand using the clipped nylon cloth. After that, the steps involving the PCBM

solution preparation until the device performance measurement follow those of unrubbed devices.

The thickness and surface roughness of ADP and AND P3HT films were measured using Keyence VN-8000 Atomic Force Microscope (AFM). The element mapping of the ADP and AND P3HT/PCBM devices was performed using energy-dispersive X-ray spectroscopy (EDS) integrated with JEOL JEM-ARM20F scanning transmission electron microscope. The evaluation of molecular orientation in ADP and AND P3HT films were accomplished using Thermo Fisher Scientific Nicolet 6700 Fourier-transform infrared spectroscopy (FTIR) equipped with an automatic pMAIRS equipment. Through these characterizations, the effect of rubbing and annealing on the active layer nanomorphology is thoroughly differentiated and correlated with PV characteristics of the BL P3HT/PCBM OSCs.

4.3 Results and Discussion

4.3.1 Photovoltaic Performance of Reproducible Unrubbed P3HT/PCBM OSCs

Fig. 4.1 shows the *J-V* curves of three unrubbed devices, fabricated at similar conditions as described in the experimental procedures (Section 4.2.1). These devices are denoted as Devices A, B and C. The photovoltaic characteristics consisting of J_{sc}, V_{oc}, *FF* and *PCE* are shown in Table 4.1 and Fig. 4.2. The J_{sc}, V_{oc}, *FF* of each device are comparable to each other, yielding ca. 1 % *PCE*. The *J-V* curves of all AND devices are almost exactly similar, indicating their similar J_{sc}, V_{oc} and *FF*. The huge increments of these PV parameters in AND devices yield ca. 2.9% *PCE*.

As discussed in Chapter 2 (Section 2.3.4), the use of high Al evaporation rate (ca. 7 Å/s) ensures the formation large grain size of Al electrode for better electron collection.[7,8] Apart from that, there are several contributing factors to these decent devices. Initially, it was speculated that the PEDOT:PSS layer that has been deposited for long time (not fresh) may

degrade, resulting in low *FF* of the device. Thus, during the experiment, the P3HT solution was prepared first, followed by substrates cleaning and PEDOT:PSS spin-coating. The samples were immediately transferred to glove box after depositing the PEDOT:PSS layers. Then, the PV performance evaluation was immediately performed after the device fabrication to avoid the device degradation. Apart from that, the use of 4 mm^2 square mask instead of the usual 2 mm^2 rectangular mask during Al evaporation helps to reduce the overestimation of device performance evaluation due to the larger area of each pixelated cell. On the other hand, the PCBM solution was prepared just before its deposition to avoid its evaporation and maintain its concentration.

In case of the heat treatment, before performing the post-annealing process, thermocouple was used to validate the temperature of the top surface of hot plate. It is found there is temperature difference at ± 4 °C depending upon the area of hot plate. The devices were put exactly at the spots having the closest temperature to 140 °C (i.e. ± 1 °C). Lastly, as the CB solvent has low boiling point (132 °C), the bottle was tightened and sealed with paraffin film to avoid the solution evaporation (i.e. reduction of solution concentration) throughout the P3HT solution stirring process.

The consistent application of these additional steps during the device fabrication has led to reproducible PV performance of BL P3HT/PCBM OPV devices. The reproducibility of the performance of unrubbed device envisages the possibility to fabricate the rubbed devices with reproducible performance.

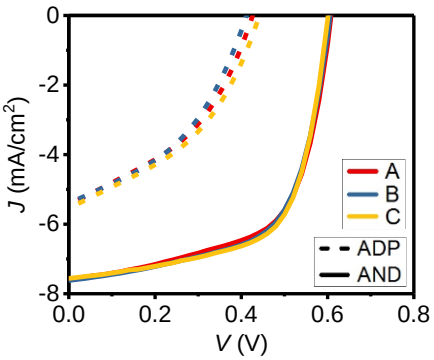

Figure 4.1. *J-V* curves of unrubbed bilayer P3HT/$PC_{61}BM$ OPV devices.

Table 4.1. PV characteristics of unrubbed BL P3HT/PCBM OPV devices.

Device	J_{sc} (mA/cm^2)		V_{oc} (V)		*FF*		*PCE* (%)	
	ADP	AND	ADP	AND	ADP	AND	ADP	AND
A	5.42	7.59	0.43	0.61	0.41	0.61	0.95	2.83
B	5.40	7.63	0.42	0.61	0.42	0.62	0.94	2.86
C	5.53	7.57	0.44	0.60	0.41	0.64	1.01	2.91

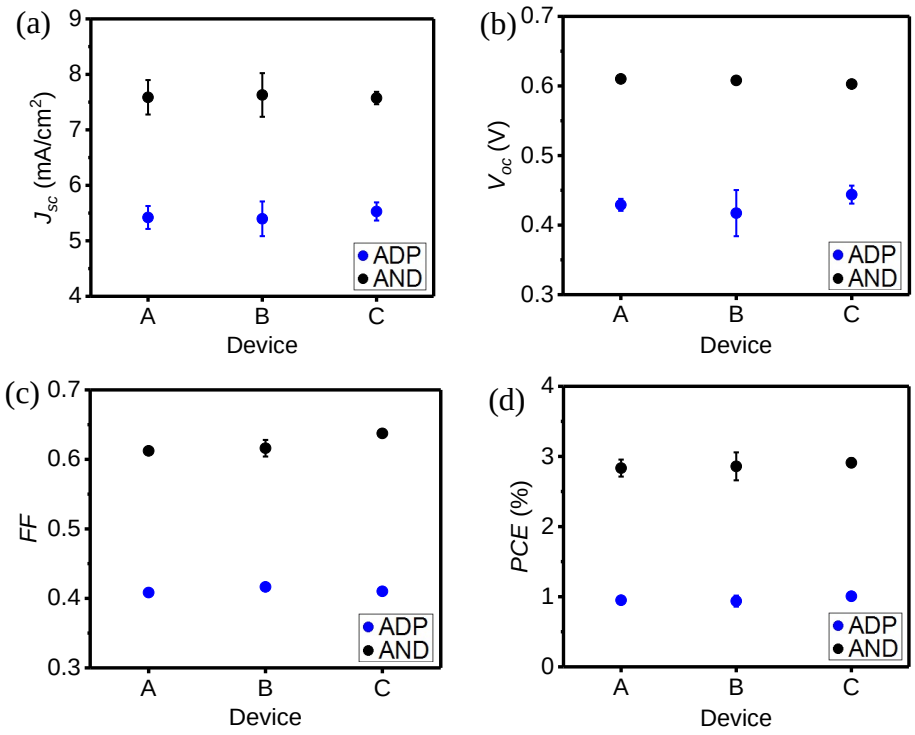

Figure 4.2. Photovoltaic performance of unrubbed bilayer P3HT/$PC_{61}BM$ OPV devices: (a) short-circuit current density, J_{sc}, (b) open-circuit potential, V_{oc}, (c) fill factor, *FF* and (d) power conversion efficiency, *PCE*.

4.3.2 Photovoltaic Performance of Rubbed P3HT/PCBM OSCs

Effect of rubbing on J_{sc}, V_{oc} and *FF* of the ADP and AND BL P3HT/PCBM OSCs is shown in *J-V* curves (Fig. 4.3). The quantitative comparison of the PV characteristics from all the devices including their *PCE* was provided by Table. 4.2 and Fig. 4.4. The increase of rubbing number significantly enhances J_{sc}, V_{oc} and *FF* in 5 times rubbed ADP device, leading to its prominent increase of the average *PCE*. Further increase of rubbing number up to 20 times, however, decreases the PV characteristics of the devices. Upon annealing, the devices show enhanced charge carrier extraction as exhibited by the improved V_{oc} and *FF* values. This results in less striking increments of the PV characteristics in the rubbed AND devices. Particularly, there is almost no change of J_{sc} and V_{oc} with the increase of rubbing number up to 20 times in AND OSCs. The *PCE* slightly improves up to 10 times rubbed device mainly due to the increase of *FF* from 0.62 to 0.66. The application of rubbing beyond 10 times results in the slight decrease of *PCE* as *FF* decreases to 0.63. It can be observed from the PV characteristics of ADP and AND devices that V_{oc} and *FF* are the major factors that proportionally influence the performance of respective ADP and AND devices.

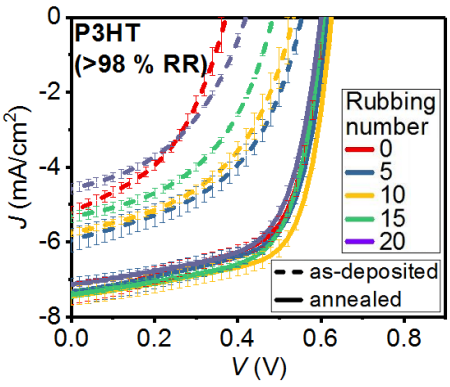

Figure 4.3. *J-V* curves under illumination of as-deposited and annealed bilayer P3HT/PCBM OPV devices with different rubbing times.

Table 4.2. Average photovoltaic characteristics of as-deposited and annealed bilayer P3HT/PCBM OPV devices at different rubbing numbers.

Rubbing number	J_{sc} (mA/cm^2)		V_{oc} (V)		*FF*		*PCE* (%)	
	ADP	AND	ADP	AND	ADP	AND	ADP	AND
0	5.19±0.14	7.37±0.30	0.37±0.01	0.61±0.00	0.43±0.01	0.62±0.01	0.83±0.03	2.78±0.09
5	5.94±0.32	7.33±0.36	0.56±0.01	0.62±0.00	0.48±0.00	0.63±0.02	1.58±0.11	2.86±0.09
10	5.75±0.08	7.45±0.25	0.54±0.01	0.63±0.00	0.48±0.01	0.66±0.00	1.47±0.07	3.09±0.11
15	5.33±0.14	7.40±0.10	0.48±0.01	0.60±0.01	0.46±0.01	0.63±0.01	1.21±0.03	2.89±0.02
20	4.48±0.12	7.14±0.08	0.41±0.02	0.60±0.00	0.43±0.00	0.63±0.01	0.83±0.01	2.70±0.07

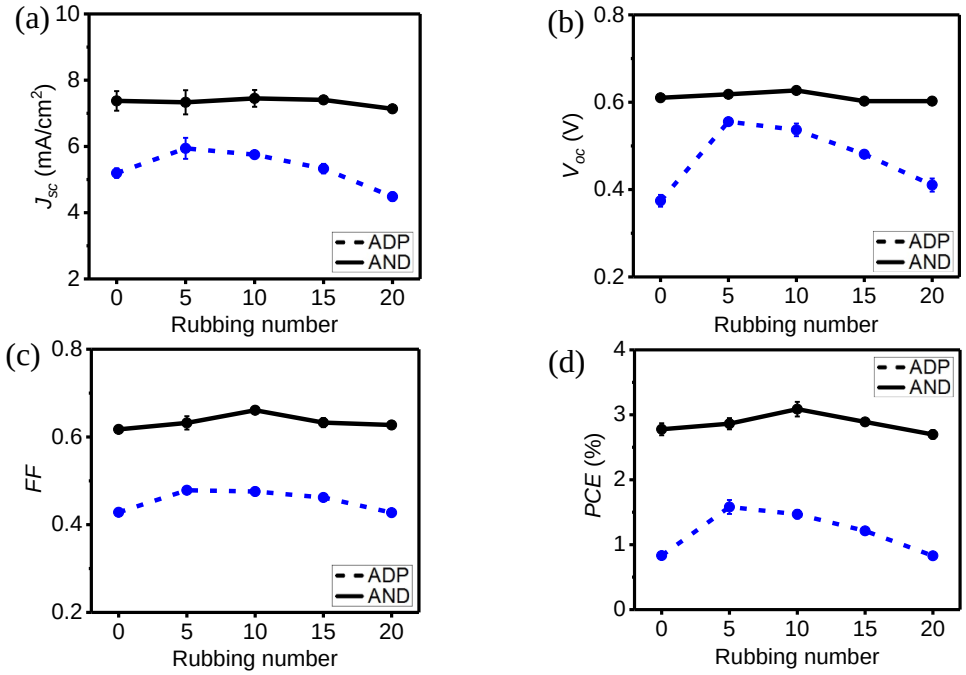

Figure 4.4. Photovoltaic performance of bilayer P3HT/PCBM OPV devices: (a) J_{sc}, (b) V_{oc}, (c) *FF* and (d) *PCE* of ADP and AND P3HT/PCBM devices with different rubbing numbers.

4.3.3 Morphological, Compositional and Structural Properties of Unrubbed and Rubbed Active Layers

The subsequent results of morphological, compositional and structural characterizations reveal the reasons behind the influence of rubbing on the PV performances of the ADP and AND BL P3HT/PCBM devices. Rubbing locally get rid of P3HT from the surface of the deposited P3HT layers and therefore a P3HT thickness reduction can be found with the increase of rubbing number (Table 4.3). As the thin P3HT films would have low series resistance, efficient hole

collection in BL P3HT/PCBM devices is expected. Nevertheless, further decrease of P3HT layer thickness generally results in increased leak currents because of the high chance for PCBM molecules to gradually diffuse inside the P3HT layer. Therefore, the excessive thickness reduction of the P3HT layers could result in detrimental impact on the *FF* of BL P3HT/PCBM OSCs. The unrubbed P3HT/PCBM devices have already being optimized in terms of P3HT thickness to achieve the highest possible *FF* and *PCE*. Even though it is undeniable that the P3HT thickness reduction could contribute to the increased *FF* on the rubbed devices, the minor change in P3HT thickness (within 2.5 nm up to 10 rubbing times) should not significantly affect the PV performances of the rubbed BL devices.

Table 4.3: Thickness and surface roughness of ADP P3HT and P3HT/PCBM films with 0-20 rubbing numbers.

Rubbing number	Thickness (nm)		R_y (nm)
	P3HT	P3HT/PCBM	P3HT
0	46.8±0.6	58.5±0.8	22.5±6.9
5	45.4±0.3	52.3±1.8	19.8±6.8
10	44.3±0.4	49.1±0.2	13.5±1.2
15	43.5±0.1	46.2±0.1	15.7±1.5
20	43.2±0.7	43.0±0.5	21.1±3.5

The localized removal of P3HT also generates uniaxial grating-like topographies on the rubbed surfaces as presented in Fig. 4.5. Such morphological changes affect the surface roughness of P3HT films depending upon the rubbing number. Based on the maximum height of the topographic profile (R_y), while rubbing up to 10 times gradually reduces the R_y of ADP P3HT film from 22.5 to 13.5 nm, further increase of rubbing number up to 20 times results in the increase of R_y from 13.5 to 21.1 nm, a comparable value to that of unrubbed film (22.5 nm). Having said that, the deposition of ca, 24 nm thick PCBM on these P3HT films may overly inter-diffuse the PCBM and P3HT films. The changes of the thickness and surface roughness of P3HT films are predicted to change the degree of PCBM diffusion into the ADP P3HT layer.

By disregarding the PCBM diffusion into the underlying P3HT layer, the sequential deposition of 24 nm thick PCBM into 47 nm thick P3HT would bring about the combined value of 71 nm BL P3HT/PCBM. The fact that the unrubbed P3HT/PCBM BL is 58.5 thick confirmed that PCBM molecules penetrate into the P3HT layer. The increase of rubbing number gradually reduces the thickness of P3HT layers from 46.8 nm to 43.2 nm. The impact of rubbing on the BL is more significant compact to this small thickness reduction. As for 10 times-rubbed P3HT layers, the thickness reduction is by 2.5 nm with respect ot the unrubbed films. However, the resulting BLs demostrate a large thickness difference of ca. 10 nm. It is worth to note that the 20 times-rubbed P3HT films and BLs have a comparable thickness (43 nm), suggesting that PCBM molecules diffuse entirely within the underlying P3HT layer.

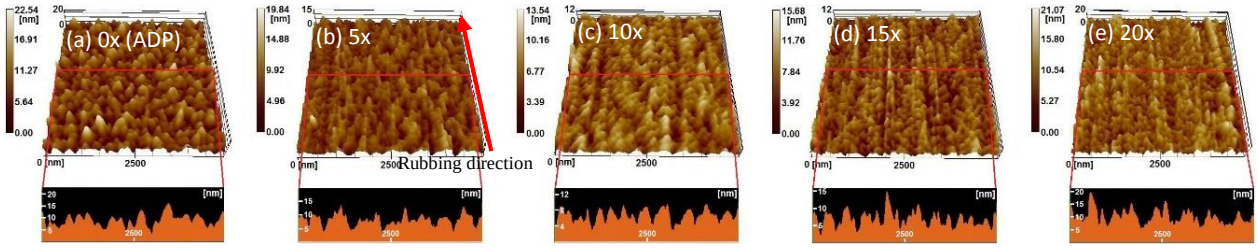

Figure 4.5. AFM images of ADP P3HT films corresponding to (a) 0, (b) 5, (c) 10, (d) 15 and (e) 20 times rubbing. Each image corresponds to an area of 5 μm × 5 μm.

In addition to the morphological and optical features of individual P3HT layers, it is essential to have the clear image of the whole device cross section to correlate the enhanced PV characteristics by rubbing the P3HT films. In this regard, the EDS elemental mapping was performed on the ADP and AND P3HT/PCBM OPV devices (Fig. 4.6) to estimate the amount of PCBM diffusing into the P3HT layers. The detected elements [blue: indium (In), green: sulfur (S), black: carbon (C) and red: Al] display the distinctive layers within the devices having glass/ITO/PEDOT:PSS(39 nm)/P3HT/PCBM BLs(40-60 nm)/Al(100 nm) configuration. Since P3HT contains sulfur, the change of the sulfur profiles (white line in Fig. 4.6) within 50-90 nm region indicates the location of P3HT in the active layer. For the region

of 80-120 nm, the detected sulfur is from PEDOT:PSS layer. The cross-section of unrubbed ADP device in Fig. 4.6a indicates significant amount of P3HT layer exists beside the Al electrode. This brings about charge recombination within that region that lowers its V_{oc}[9,10] (Fig. 4.4b). By rubbing the P3HT layer, P3HT near Al electrode disappeared (Figs 4.6b-e). This change effectively reduces charge recombination in rubbed ADP devices. In 5 times rubbed ADP device, the significant decrease of P3HT concentration near to Al significantly increases its V_{oc} from 0.37 to 0.56 V. By looking at Fig. 4.6b, the formation of considerably large intermixed layer between 40-70 nm enhances charge generation and transport. Consequently, J_{sc} and *FF* increase from 5.19 to 5.94 mA/cm^2 and 0.43 to 0.48 respectively. Further increase of rubbing number up to 15 times (Fig. 4.6d) indicates the deeper diffusion of PCBM nearer to PEDOT:PSS region which in turn substantially reduces the V_{oc} from 0.54 V (10 times rubbed device) to 0.48 V (15 times rubbed device) due to recombination loss.[11] The disappearance of intermixed layer in 15 times rubbed device indicates lower charge generation and transport that explain the reduced J_{sc} and *FF* from 5.75 mA/cm^2 and 0.48 (10 times rubbed device) to 5.33 mA/cm^2 and 0.46 (15 times rubbed device). Despite of identical sulfur profiles between 15 times and 20 times rubbed devices, the significant reduction of active layer thickness in 20 times rubbed device limits the exciton formation.[12] As a result, its V_{oc}, J_{sc} and *FF* decrease to 0.41 V, 4.48 mA/cm^2 and 0.43 respectively. In this regard, the excessive rubbing causes PCBM to overly diffuse into P3HT layer and reduces the thickness of P3HT, complying with the AFM image in Fig. 4.5e. The compositional studies of ADP devices shows that the composition of active layer and the presence of intermixed layer strongly depend on the rubbing number in which rubbing provides a simple solution to avoid the formation of a P3HT-rich layer at the top interface (Figs. 4.6a-e) before undergoing thermal annealing heat treatment. It is found that the adequate vertical profiles are formed when P3HT films are rubbed 5 or 10 times before PCBM deposition.

As for the AND devices, the PCBM and P3HT layers aggregated to form distinctive active layers that reflect the modification of the vertical concentration profiles.[3,13–15] The cross sections of ADP and AND devices show that PCBM molecules aggregate at the top interface of the active layers next to Al electrode (Figs 4.6f-j), matching with the findings on the impact of annealing on the active layer nanomorphology.[14,15] In ADP unrubbed active layers, there is P3HT-rich layer in contact with the top Al electrode, but upon thermal annealing and the diffusion of the PCBM molecules at the top interface, the P3HT-rich layer is confined towards the center of the AND active layers as shown in Fig. 4.6f. The nanoscale phase segregated layers produced in AND condition can considerably reduce recombination losses and simultaneously enhanced charge transport.[11,13] Having the ideal vertical concentration gradients, the PV characteristics dramatically enhance in unrubbed AND device: V_{oc} (from 0.37 to 0.61 V), J_{sc} (from 5.19 to 7.37 mA/cm^2) and *FF* (from 0.43 to 0.62). Such increase of V_{oc} is due to the reduced recombination losses. On the other hand, more efficient charge transport resulting from the adequate concentration gradients and partial crystallization of the active layers through aggregation contribute to such enhancements of J_{sc} and *FF*. Similarly to unrubbed AND layers, P3HT-free top interfaces are formed in AND BLs rubbed 5 or 10 times. Rubbing from 5 to 20 times is found to separate the P3HT away from Al and simultaneously form large intermixed P3HT:PCBM layers having intimately mixed electron donor and electron donor materials within 40-90 nm region (Figs. 4.6g-j). These layers further enhance the charge generation within the active layer.[11,12] These observations match with the PV performance of the AND OSCs in Table 4.2. The absence of P3HT near to Al and the presence of large intermixed layer contribute to the highest V_{oc} (0.63 V), J_{sc} (7.45 mA/cm2) and *FF* (0.66) in 10 times rubbed device. The decrease performance in 15 and 20 times rubbed devices are due to the presence of a small amount of P3HT near to Al that results in charge recombination. The compositional studies of AND devices indicate that annealing leads to large improvements in PV performances of BL P3HT/PCBM devices through the formation of

a top interface that is free from P3HT, promoting efficient electron collection at the Al electrode and inducing active layer crystallization. Nevertheless, the active layer composition in the bulk and at the buried interface is not strongly influenced by thermal annealing. Additionally, rubbing slightly alters the composition of active layer near to Al electrode with a small influence on the intermixed layer of AND BLs. These findings explain the reason behind the less influence of rubbing on the PV characteristics of AND devices as compared to those of ADP devices (Fig. 4.4).

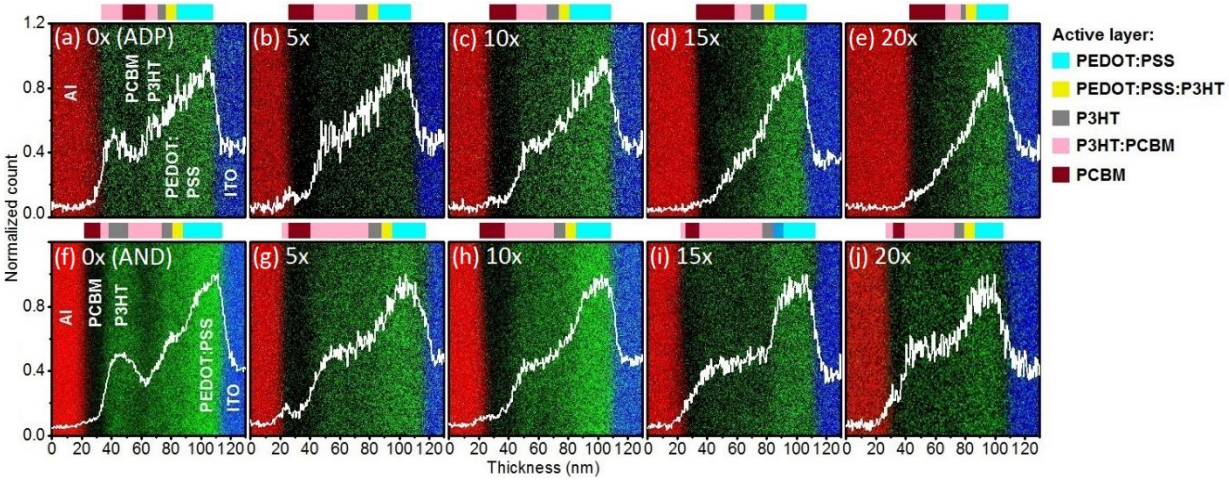

Figure 4.6. The cross-sectional EDS element mappings of ADP P3HT/PCBM devices corresponding to (a) 0, (b) 5, (c) 10, (d) 15 and (e) 20 times rubbing; and AND P3HT/PCBM devices corresponding to (f) 0, (g) 5, (h) 10, (i) 15 and (j) 20 times rubbing. The detected elements are indium (blue), sulfur (green), carbon (black) and aluminum (red). The white line represents the normalized sulfur profile. The color scales above the EDS images indicate the estimated active layer composition based on the normalized sulfur profiles.

Apart from the active layer thickness, morphology and concentration gradient of active layer, another factor that could influence the charge transport efficiency is the orientation of P3HT molecules where the face-on molecules with the thiophene ring lying parallel to the substrate facilitates the charge transport to the electrodes.[4,5] To investigate the influence of rubbing on the molecular orientation at the surface of P3HT layer, pMAIRS measurements are performed on the P3HT films prepared with increasing rubbing number. This characterization

may be the adequate technique to probe unrubbed and rubbed P3HT-based samples as it provides information on molecular orientation for each chemical group irrespective of the thin film crystallinity.[16,17] The in-plane (IP) and out-of-plane (OP) infrared (IR) absorbance spectra of P3HT and P3HT/PCBM films were generated from pMAIRS measurement at a refractive index (n) of 1.6 for P3HT[18] as shown in Figs. 4.7a-d. The thiophene ring vibration [ν(C=C)] mode appears at ca. 1510 cm^{-1}wavenumber while the C-H out-of-plane deformation vibration [γ(C-H)] mode on the thiophene ring is observed at ca. 820 cm^{-1}.[19,20]

The transition moments of ν(C=C) and γ(C-H) modes serve as an indicator to estimate the molecular orientation of P3HT molecules.[21] The polymer chain is parallel to the transition moment of ν(C=C) mode while the thiophene ring is perpendicular to that of γ(C-H) mode.[20,21] By taking into account the absorbance (band intensities) in OP spectrum (A_{OP}) and the absorbance in IP spectrum (A_{IP}), the orientation angle (ϕ) can be calculated using the following equation.[22]

$$\phi = tan^{-1}\sqrt{\frac{2A_{IP}}{A_{OP}}} \tag{5.1}$$

The pMAIRS spectra of unrubbed film exhibit the presence of dominant ν(C=C) and γ(C-H) bands in the IP spectrum with the measured orientation angle of γ(C-H) mode from the surface normal, $\phi_{C\text{-}H}$ = 68°, indicating the edge-on molecular orientation.[20] Interestingly, by looking at 5 times rubbed spectra, the OP peak appears at 821 cm^{-1} [γ(C-H)] where rubbing is found to align the P3HT molecules to $\phi_{C\text{-}H}$ = 63°. Further increase of rubbing number slightly increases the γ(C-H) OP peaks, reducing $\phi_{C\text{-}H}$ to 52° on 20 times rubbed film (Fig. 4.7a). Typically, pMAIRS generates measurement deviations of ±5°,[23] thus the notable molecular orientation angle should be considered once the changes in $\phi_{C\text{-}H}$ are greater than 10°. Nonetheless, the changes of $\phi_{C\text{-}H}$ in ADP P3HT films indicate that the P3HT molecules are

gradually aligned towards face-on orientation with the increase of rubbing number. Meanwhile, there are comparable intensities of ν (C=C) and γ (C-H) modes in IP spectra of the corresponding AND P3HT films where the $\phi_{\text{C-H}}$ of AND films are equivalent with those of respective ADP films (Figs. 4.7c and e). This implies that annealing does not significantly change the orientation of P3HT molecules in P3HT single layer.

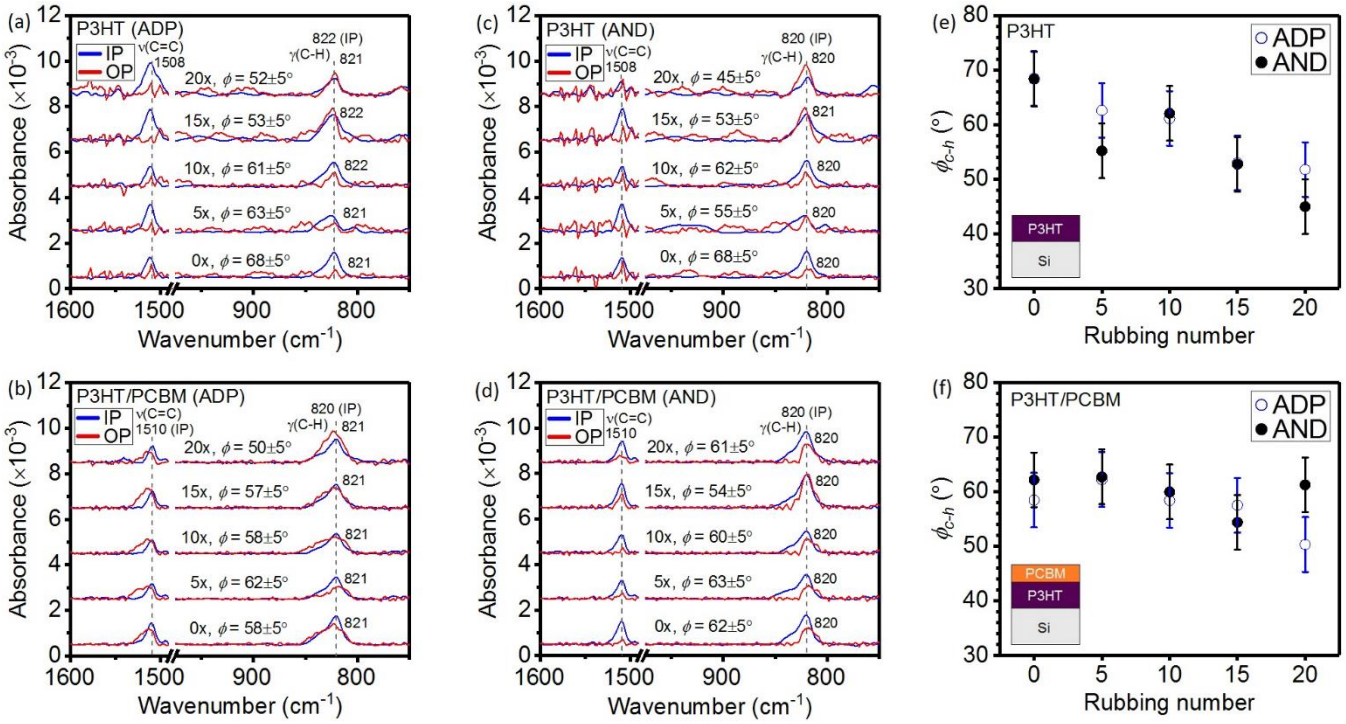

Figure 4.7. The IR pMAIRS absorbance spectra of ADP (a) P3HT and (b) P3HT/PCBM films along with AND (c) P3HT and (d) P3HT/PCBM films with different rubbing times on P3HT films; the orientation angles of (e) P3HT and (f) P3HT/PCBM films are calculated from the absorbance spectra in ADP and AND conditions having different rubbing times on P3HT films. The typical error bar for the orientation angles is ±5°.

Deposition of the PCBM upper layer can extensively affect the orientation of P3HT molecules on the surface of P3HT films. Hence, pMAIRS measurements are carried out on ADP and AND P3HT/PCBM BLs in order to understand if the improved performances observed in rubbed P3HT/PCBM devices can be correlated with molecular orientation. It is found that the unrubbed ADP and AND P3HT/PCBM BLs display the $\phi_{\text{C-H}}$ values of 58° and

62°, respectively (Figs. 4.7b and d). The small difference between $\phi_{C\text{-}H}$ values of P3HT single layers and P3HT/PCBM BLs suggests that the deposition of PCBM layer does not significantly affect the molecular orientation in unrubbed P3HT films (Figs. 4.7e and f). By rubbing the P3HT films up to 15 times, ADP BLs exhibit $\phi_{C\text{-}H}$ values between 57° and 62° (Figs. 4.7b and f), indicating that the large *FF* increments in ADP BL OSCs rubbed up to 15 times cannot be attributed to molecular orientation in the P3HT layer (Table 4.2). As for the AND BLs, the band intensities of the OP peaks remain almost unchanged where $\phi_{C\text{-}H}$ seems steady regardless of the rubbing number (Fig. 4.7d) with the measured values between 54° and 61°. Similarly to the case of ADP BLs, such small variations of $\phi_{C\text{-}H}$ in AND BLs cannot be correlated with the notable *FF* increases found in rubbed AND BLs OSCs. pMAIRS measurements of P3HT single layer and P3HT/PCBM BLs in both ADP and AND conditions strongly imply that the slight change of molecular orientation upon rubbing plays a less significant role than the formation of adequate concentration gradients to be correlated with the PV performance of BL P3HT/PCBM OSCs.

4.4 Summary

The careful experimental handling with the consideration of the optimization of device fabrication procedures realize the reproducible P3HT/PCBM OPV devices. The proper control of PCBM diffusion into P3HT layer results in significant increase of *PCE* in ADP devices from 0.83% (unrubbed) to 1.58% (5 times rubbed). In unrubbed devices, the phase segregation of PCBM layer at the top interface of the photoactive layer resulting from annealing brings about a significant increase of *PCE*, from 0.83% (ADP) to 2.78%% (AND). The synergy of rubbing and annealing further increases the *PCE* from 2.78% (unrubbed) to 3.09% (10-times rubbed). The experimental results clearly show that rubbing P3HT layer before PCBM deposition

substantially affects the nanomorphology of the resulting active layers. Particularly, rubbing the ADP active layers brings about sufficient vertical concentration gradients. Annealing heat treatment further enhances the concentration profiles of the rubbed BLs by forming the equally mixed interlayers capped with PCBM buffer layers. Despite the lack of edge-on to face-on molecular orientation in P3HT/PCBM BLs, the higher *FF* measured in rubbed AND OSCs compare to that of ADP devices confirms that the adequate concentration profiles strongly affect the charge extraction properties of the BL OSCs. The interfacial and bulk properties acquired from the morphological and compositional analyses consequently indicate the importance of controlling the vertical concentration gradient of the photoactive layer to realize high PV performances of the devices in both ADP and AND conditions.

4.5 References

1) S.A. Hawks, J.C. Aguirre, L.T. Schelhas, R.J. Thompson, R.C. Huber, A.S. Ferreira, G. Zhang, A.A. Herzing, S.H. Tolbert, and B.J. Schwartz, J. Phys. Chem. C **118**, 17413 (2014).
2) J.S. Moon, C.J. Takacs, Y. Sun, and A.J. Heeger, Nano Lett. **11**, 1036 (2011).
3) K.H. Lee, P.E. Schwenn, A.R.G. Smith, H. Cavaye, P.E. Shaw, M. James, K.B. Krueger, I.R. Gentle, P. Meredith, and P.L. Burn, Adv. Mater. **23**, 766 (2011).
4) V. Vohra, G. Arrighetti, L. Barba, K. Higashimine, W. Porzio, and H. Murata, J. Phys. Chem. Lett. **3**, 1820 (2012).
5) D. Kajiya, S. Ozawa, T. Koganezawa, and K.I. Saitow, J. Phys. Chem. C **119**, 7987 (2015).
6) L. Hartmann, K. Tremel, S. Uttiya, E. Crossland, S. Ludwigs, N. Kayunkid, C. Vergnat, and M. Brinkmann, Adv. Funct. Mater. **21**, 4047 (2011).
7) T.S. Glen, N.W. Scarratt, H. Yi, A. Iraqi, T. Wang, J. Kingsley, A.R. Buckley, D.G. Lidzey, and A.M. Donald, J. Polym. Sci. Part B Polym. Phys. **140**, 25 (2015).
8) K. Bordo and H.G. Rubahn, Mater. Sci. **18**, 313 (2012).
9) B.G. Kim, E.J. Jeong, H.J. Park, D. Bilby, L.J. Guo, and J. Kim, ACS Appl. Mater. Interfaces **3**, 674 (2011).
10) S.B. Hacène and T. Benouaz, Phys. Status Solidi Appl. Mater. Sci. **211**, 862 (2014).
11) V.S. Gevaerts, L.J.A. Koster, M.M. Wienk, and R.A.J. Janssen, ACS Appl. Mater. Interfaces **3**, 3252 (2011).
12) H. Ohkita and S. Ito, Polymer **52**, 4397 (2011).
13) K.A. Mazzio and C.K. Luscombe, Chem. Soc. Rev. **44**, 78 (2014).
14) V. Vohra, N.T. Razali, and H. Murata, in Sci. Appl. Tailored Nanostructures, edited by P. Di Sia, 1st ed. (One Central Press, Manchester, UK, 2017), pp. 128–147.

15) A. Orimo, K. Masuda, S. Honda, H. Benten, S. Ito, H. Ohkita, and H. Tsuji, Appl. Phys. Lett. **96**, 043305 (2010).

16) N. Shioya, R. Murdey, K. Nakao, H. Yoshida, T. Koganezawa, K. Eda, T. Shimoaka, and T. Hasegawa, Sci. Rep. **9**, 579 (2019).

17) T. Hasegawa and N. Shioya, Bull. Chem. Soc. Jpn. (2020).

18) N. Shioya, T. Shimoaka, R. Murdey, and T. Hasegawa, Appl. Spectrosc. **71**, 1242 (2017).

19) N. Shioya, T. Shimoaka, K. Eda, and T. Hasegawa, Phys. Chem. Chem. Phys. **17**, 13472 (2015).

20) N. Shioya, T. Shimoaka, K. Eda, and T. Hasegawa, Macromolecules **50**, 5090 (2017).

21) N. Shioya, T. Shimoaka, and T. Hasegawa, Chem. Lett. **43**, 1198 (2014).

22) N. Shioya, M. Hada, T. Shimoaka, R. Murdey, K. Eda, and T. Hasegawa, J. Phys. Chem. C **122**, 4540 (2018).

23) T. Hasegawa, J. Phys. Chem. B 106, 4112 (2002).

Chapter 5

CONCLUSION AND FUTURE WORKS

5.1 Conclusion

Rubbing technique has been developed and applied specifically on bilayer OPV devices using the prototypical P3HT and PCBM for the electron donor and electron acceptor materials, respectively. The initial fabrication and characterizations of unrubbed the bilayer P3HT/PCBM OPV devices and P3HT film samples lead to the deeper understanding on the properties of the active layer before and after applying the post-annealing heat treatment. The optimization process of unrubbed devices has narrowed down the device fabrication parameters where the substrate cleaning, electron acceptor, P3HT solvent, heat treatment and the evaporation rate of Al electrode were optimized. The development of rubbing process from the simple folded nylon cloth brings about the quantitative control the rubbing pressure via the automatic rubbing device. Since the control of the rubbing pressure is not reproducible, the folded nylon cloth was reused with the clip to ensure the consistency of the rubbing pressure. This minor development of manual rubbing has shown fruitful results together with the reproducibility of the photovoltaic performance of rubbed and unrubbed devices. We have found that the use of simple rubbing technique with the very careful control of the experimental procedures are the key to achieve the decent performance of bilayer P3HT/PCBM OPV devices. The use of the clipped nylon cloth enables the variation of rubbing number at consistent rubbing pressure on P3HT films. The morphological, compositional and structural studies reveal the individual effects of rubbing and annealing on the PV performances of as-deposited and annealed devices. Rubbing P3HT layer prior to PCBM deposition leads to sufficient vertical concentration gradients in ADP BL P3HT/PCBM OSCs while annealing further enhances the concentration

profiles of the rubbed BLs by forming the equally mixed interlayers. Structural studies infer that the slight change of molecular orientation upon rubbing plays a less significant role than the formation of adequate concentration gradients to be correlated with the PV performance of BL devices. The characterizations carried out throughout the research point out the significance of controlling the vertical concentration gradient of the photoactive layer in order to realize the BL OSCs having the decent PV performances.

5.2 Future Works

The development of automatic rubbing device was not completely successful as the steady increments of PV parameters in rubbed devices could not be attained. However, it managed to emphasize the rubbing pressure as the important rubbing parameters in addition to the so-called rubbing number. The careful enhancement on the control of rubbing parameter in term of the tilting angle between the P3HT film sample and the nylon cloth, may possibly overcome the current drawback of the automatic rubbing device. The application of rubbing using the simple rubbing method (i.e. clipped nylon cloth) on the high RR-P3HT has pointed out the influence of the P3HT regioregularity on the PV performance of the rubbed bilayer device. We hereby propose that the rubbing process on the P3HT film with the optimized RR could be able to achieve better device performance than our current device performances. The optimization of P3HT can be done by mixing the high RR-P3HT with either low RR-P3HT or regiorandom (RRa) P3HT. We believe that the current record of the efficiency of bilayer P3HT/PCBM OPV devices can be overcome by thoroughly applying the aforementioned suggestions.

On the other hand, evaluating whether the sufficient concentration profiles are formed prior to annealing is a deciding factor to expand the application of rubbing to other donor/acceptor systems. As rubbing was found to induce adequate donor/acceptor segregation in the BL OSC active layers, the use of rubbing could possibly be extended donor/acceptor systems based on

low bandgap copolymers or non-fullerene acceptors that do not need high temperature heat treatment above 100°C. Thus, the findings on the individual impacts of rubbing and annealing could open the path to highly efficient and air-stable OSC fabrication.